Journal of Computational Physics 229 (2010) 760–787

Contents lists available at ScienceDirect

Journal of Computational Physics

journal homepage: www.elsevier.com/locate/jcp

The Riemann Problem for the one-dimensional, free-surface Shallow Water Equations with a bed step: Theoretical analysis and numerical simulations

G. Rosati *, L. Begnudelli

Centro Universitario per la Difesa idrogeologica dell'Ambiente Montano (CUDAM), Dipartimento Ingegneria Civile e Ambientale, Università degli Studi di Trento, Via Mesiano, 77, 38050 Trento, Italy

ARTICLE INFO

Article history:
Received 16 June 2009
Received in revised form 6 October 2009
Accepted 7 October 2009
Available online 13 October 2009

Keywords:
Bed discontinuity
Shallow Water Equations
Riemann Problems
Nonconservative systems
Contact waves
Generalized Roe solver

ABSTRACT

In this paper, the solution of the Riemann Problem for the one-dimensional, free-surface Shallow Water Equations over a bed step is analyzed both from a theoretical and a numerical point of view. Particular attention has been paid to the wave that is generated at the location of the bed discontinuity. Starting from the classical Shallow Water Equations, considering the bed level as an additional variable, and adding to the system an equation imposing its time invariance, we show that this wave is a contact wave, across which one of the Riemann invariants, namely the energy, is not constant. This is due to the fact that the relevant problem is nonconservative. We demonstrate that, in this type of system, Riemann Invariants do not generally hold in contact waves. Furthermore, we show that in this case the equations that link the flow variables across the contact wave are the Generalized Rankine–Hugoniot relations and we obtain these for the specific problem. From the numerical point of view, we present an accurate and efficient solver for the step Riemann Problem to be used in a finite-volume Godunov-type framework. Through a two-step predictor–corrector procedure, the solver is able to provide solutions with any desired accuracy. The predictor step uses a well-balanced Generalized Roe solver while the corrector step solves the exact nonlinear system of equations that consitutes the problem by means of an iterative procedure that starts from the predictor solution. In order to show the effectiveness and the accuracy of the proposed approach, we consider several step Riemann Problems and compare the exact solutions with the numerical results obtained by using a standard Roe approach far from the step and the novel two-step algorithm for the fluxes over the step, achieving good results.

© 2009 Elsevier Inc. All rights reserved.

1. Introduction

In many practical problems involving free-surface shallow-flows, the effects of bed discontinuities on hydrodynamics are key features that a good numerical model must be able to deal with, achieving the same level of accuracy as elsewhere. We are not talking about discontinuities deriving from the discretization of the bed elevation, but about all the real discontinuities that can be found in overland flows: dams, check-dams, sills and any other obstacle that can act as a bed step (e.g. vertical underpasses, walls, and so on). In particular, we are interested in dealing with this problem in the framework of finite-volume, Godunov numerical schemes. Since the key ingredient of this approach consists in finding the exact or approximated solution of a Riemann Problem (RP), in the present work we are interested in the RP that develops across a bed step.

* Corresponding author. Tel.: +39 0461882621; fax: +39 0461882672.
E-mail addresses: giorgio.rosatti@ing.unitn.it (G. Rosatti), lorenzo.begnudelli@ing.unitn.it (L. Begnudelli).

0021-9991/$ - see front matter © 2009 Elsevier Inc. All rights reserved.
doi:10.1016/j.jcp.2009.10.010

We refer to this specific RP as a Step Riemann Problem (SRP). Despite the fact that this topic is not new and many papers have been devoted to this subject, several points regarding the exact solution of a SRP are still controversial and need to be clarified before aiming at the development of accurate numerical solvers.

What can be inferred from the literature is that, with respect to a RP on horizontal bed, the SRP presents one more standing wave positioned over the bed step, which consists in a discontinuity in the flow variables. The existence of this wave has been demonstrated in [1] on the basis of similarity considerations. On the other hand, in [6] the demonstration is obtained by using standard mathematical tools. Following the idea proposed by [11] of considering the bed level as an additional variable, the standard Shallow Water (SW) system is extended by introducing an additional equation asserting the time invariance of the bed level. The resulting system is:

$$\begin{cases} \frac{\partial h}{\partial t} + \frac{\partial}{\partial x}(hu) = 0 \\ \frac{\partial}{\partial t}(hu) + \frac{\partial}{\partial x}(hu^2 + \frac{1}{2}gh^2) + gh\frac{\partial z}{\partial x} = 0 \\ \frac{\partial z}{\partial t} = 0 \end{cases} \tag{1}$$

where h is the water depth, u is the depth-averaged velocity and z is the elevation of the bed above a reference level. In this way, the term $gh\partial z/\partial x$ is no longer a mere geometrical source term but plays an important role in the eigenstructure of the problem. A classical analysis shows that this system admits three distinct eigenvalues: two of these are the same as the classical SW equations, while the third is identically zero. The standing wave associated to this last eigenvalue is a contact wave and appears only in presence of a bed discontinuity (see Section 2.2.1 for details).

The presence of such a wave has been addressed by several works. However, the literature is controversial regarding the relations that connect the flow variables (depth and velocity) across the bed discontinuity. In particular, two approaches are present: one based on mass and energy conservation principles and the other based on mass and momentum conservation principles.

In most works, the former approach is adopted: Alcrudo et al. [1] and analogously [5] claim that the use of the mass-energy approach is compulsory because the mass-momentum approach, leading to the standard SW system (namely, system (1) without the last equation), must be discarded when the slope of the bed becomes infinite, as in a step. However, in both works there is awareness that dissipation actually occurs in the recirculation cell located at the inner corner of the step and therefore they introduce the possibility of a loss in the energy relation. Galloüet et al. [7], Chinnayya et al. [6], and Andrianov [2] claim that, since the standing wave over the step is a contact discontinuity, it must be characterized by the constancy of the relevant Riemann Invariants (RIs), namely mass and energy, in any situation except in the resonant case. This result is rather controversial because from the mathematical point of view energy losses are not admitted, while from the physical point of view it is clear that they actually exist.

In contrast, the latter approach is used in [4]. The authors, even though they initially describe the problem by means of (1), characterize the standing wave by applying the principle of conservation of mass and momentum directly to an infinitesimal control volume that includes the step, obtaining equations that can be called Generalized Rankine–Hugoniot (GRH) relations. In this work energy is used as a constraint to rule out the solutions that are physically inadmissible, i.e. those for which energy is not dissipated across the step.

The first goal of our work is to provide a unified approach, starting from system (1), able to overcome the evident contradictions between the two approaches present in the literature. A deep analysis of the features of the contact waves in nonconservative systems (as (1) appears to be) shows that, unlike in standard conservative systems, RIs are generally not constant across a contact discontinuity whose relevant eigenvalue is independent from the problem variables. In other words, it is possible to claim that system (1) admits, over the bed step, a contact wave through which energy is not conserved, while GRH relations hold. Therefore, system (1) together with the relevant GRH relations, constitutes an approach that is thoroughly exhaustive from the theoretical point of view, and also physically acceptable.

From a numerical point of view, the literature presents several different finite-volume, Godunov numerical approaches to the shallow water problem in presence of a bed step situated at the interface between two computational cells. In [24] the authors use an HLL solver for the homogeneous part of the standard SW system with a proper reconstruction of the variables (SGM method) to be used in the Riemann solver and add an eddy friction to account for the presence of the step. Galloüet et al. [7] presents several variants of Roe-type solvers applied to system (1), in which energy conservation across the contact wave is assumed. A well-balanced method, in which the SRP is solved by introducing a linear expansion of the bed step and using stationary solutions inside it, is also presented in [6]. This particular way of solving the SRP leads to solutions in which energy is preserved except in the resonant case. Finally, [15] uses a well-balanced Generalized Roe solver for nonconservative systems. Also in this case, the solver is based on constancy of the RIs across the contact wave. Summarizing, all the existent solvers use, in some way, the conservation of the energy across the step. The only exception is [4] where an exact solver based on the GRH relations is used.

Overcoming the limits of the majority of the existing solvers is the second goal of our paper. By using the GRH relations for the step contact wave, we present an SRP solver free from any bond with energy conservation. Moreover, through an efficient predictor–corrector procedure, the solver is able to provide the solution of a given SRP with any desired accuracy. The predictor step uses a well-balanced Generalized Roe solver that derives from a mobile-bed solver presented in [18]. It supplies the wave structure (the sequence and type of waves) of the SRP as well as a first estimate of the SRP solution. The corrector step solves the nonlinear system of equations related to the given wave structure by means of an iterative

Newton–Raphson method, using as a starting point for the iterations the approximate solution provided by the predictor. The proposed method has been tested against several test cases, in order to check its effectiveness and accuracy. For a number of step Riemann Problems, numerical predictions obtained by using the proposed approach have been compared to the exact solutions, obtained by an inverse procedure [2,17], achieving good results.

The paper is structured as follows: in Section (2) all the mathematical elements necessary to describe the SW problem with a bed step are presented; Section (3) is devoted to the analysis of the contact waves in nonconservative systems, while in Section (4) the corresponding relations between the flow variables are found and discussed in detail. In Section (5) the two-step solver for the SRP is presented, and in Section (6) the comparison between exact and numerical solutions (obtained using the proposed method) is presented. Finally, Section (7) closes the paper with the conclusions.

2. Mathematical description of the SW problem with a bed step

In this section, we present the derivation of all the mathematical elements necessary to describe any free-surface SW flow with (and without) the presence of a bed step. All the relations will be obtained starting from the physical principles of mass and momentum conservation written in integral form. Using this approach we give a clear physical meaning to the terms appearing in the derived equations. We first present the general formulation of the flow equations for a control volume moving with a given non-material speed. Then, from these integral equations we derive the PDEs system of the SW problem with a bed step, and the shock relations for the cases of horizontal and discontinuous bed.

2.1. Integral formulation

Let us consider a reference system with a horizontal x-axis and a vertical y-axis, with the positive direction upwards (see Fig. 1). Considering a generic two-dimensional control volume cv, moving with a non-material speed $\vec{v}_{cv}$, the principles of mass and momentum conservation read:

$$\frac{d}{dt}\int_{cv}\rho dV + \oint_{cs}(\rho)\vec{u}_r\cdot d\vec{A} = 0 \tag{2}$$

$$\frac{d}{dt}\int_{cv}(\rho\vec{u})dV + \oint_{cs}(\rho\vec{u})\vec{u}_r\cdot d\vec{A} = \sum_i \vec{F}_i \tag{3}$$

where cv and cs refer, respectively, to the control volume and to the control surface at a given time t; ρ is the density of the fluid; $\vec{u}=(u,v)$ is the fluid velocity; $\vec{u}_r=(u_r,v_r)$ is the relative velocity of the fluid with respect to the control surface; $d\vec{A}$ is a vector normal to the control surface (pointing outwards) and with module equal to dA; $\vec{F}_i$ is the ith external force acting on the control volume. Note that time derivatives are not material derivatives.

The 1D SW version of the previous equations can be obtained by introducing the following hypotheses (see e.g. [21, Chapter 10]):

(a) The control volume is defined by two vertical planes, located at $x_1(t)$ and $x_2(t)$ and moving with a non-material horizontal velocity u_0, and two material surfaces, $\Gamma_b(t)$ and $\Gamma_s(t)$, that coincide with the bed and with the free-surface, respectively (see Fig. 1); along these two surfaces, the relative velocities are null.
(b) The density ρ of the fluid is constant.
(c) The vertical fluid velocity v is negligible: the momentum conservation along the y-direction yields the hydrostatic pressure distribution.
(d) The velocity of the fluid particles is constant along any vertical section.
(e) The bed is smooth everywhere and its slope is small except for a finite number of discontinuities.

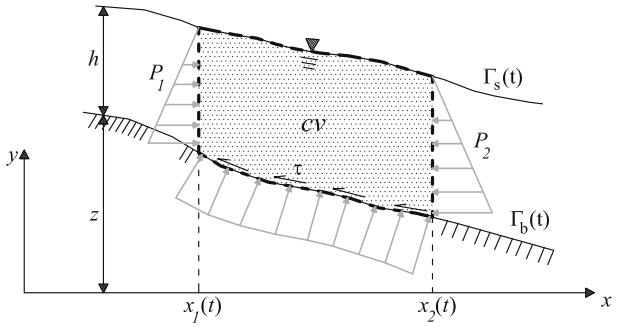

Fig. 1. Sketch of the mobile control volume cv and of the physical quantities used to derive the integral formulation of the mass and momentum conservation equations.

Notice that the point (c) can be derived more formally from the Euler equations under the hypothesis that the typical depth of the fluid is much smaller than the typical length in the horizontal direction (see [21, Chapter 2]). Moreover, it does not hold when a shallow flow occurs on a very steep bed. In these conditions it is more appropriate to assume that what is negligible is the velocity normal to the bed and not v (see e.g. [19,3]). Nevertheless assumption (e) restricts the study to cases in which point (c) is acceptable throughout the flow field.

Integral formulation of the SW equations can be obtained by using the previous assumptions and performing the integration along the y-direction of Eq. (2):

$$\frac{d}{dt}\int_{x_1(t)}^{x_2(t)} h dx + [hu_r]_{x_1(t)}^{x_2(t)} = 0 \tag{4}$$

where $[\cdot]_{x_1(t)}^{x_2(t)}$ is the difference between the value of the function inside the brackets evaluated at positions $x_2(t)$ and $x_1(t)$ and at a given time t. Analogously, the momentum conservation in the x-direction becomes:

$$\rho\frac{d}{dt}\int_{x_1(t)}^{x_2(t)} (hu) dx + \rho[(hu)u_r]_{x_1(t)}^{x_2(t)} = P_1 - P_2 + \int_{\Gamma_b(x_2(t))}^{\Gamma_b(x_2(t))} p_{bx}\, d\Gamma_b - \int_{\Gamma_b(x_1(t))}^{\Gamma_b(x_2(t))} \tau_{bx}\, d\Gamma_b \tag{5}$$

where $P_1 = \gamma h_1^2/2,\ P_2 = \gamma h_2^2/2$ ($\gamma = \rho g$ being the specific weight) are the resultants of the pressure distribution, respectively on sections $x_1(t)$ and $x_2(t)$, h_1 and h_2 are the water depths at $x_1(t)$ and $x_2(t)$ and p_{bx} and τ_{bx} are the x-components, respectively of the pressure term and the bottom stress term exerted by the bed on the fluid along $\Gamma_b(t)$.

Since we have only two equations, in order to close the problem it is necessary to provide suitable relations that link the bottom pressure and stress terms with the flow unknowns $u(x,t),\ h(x,t)$. The bed shear-stress τ_{bx} can be expressed using either the Manning or the Chézy formulation; a generic expression is the following:

$$\tau_{bx} = F(|u|, h)u$$

Nevertheless, in the rest of the paper, we have considered a frictionless bed, since the presence of the bottom friction source term does not affect the present study. As far as the bottom pressure is concerned, different assumptions must be introduced for smooth and for discontinuous-bed cases, as will be shown in the following sections.

2.2. The PDE system

The PDE system can be obtained from Eqs. (4) and (5) by using the following two assumptions (see [21]):

(a) The control volume does not move. i.e. $u_0 = 0$.
(b) The control volume is infinitesimal and inside it the flow variables are smooth functions.

The consequences of these assumptions on Eqs. (4) and (5) are the following:

1. $v_{cv} = 0,\ v_r = u;\ x_1$ and x_2 are no longer functions of time. Therefore, time derivatives become partial time derivatives;
2. using the mean-value theorem, the integrals of the variables are simply equal to the variables themselves multiplied by the infinitesimal width of the control volume;
3. under the hypothesis of hydrostatic pressure distribution, the x-component of the bottom pressure becomes:

$$p_{bx}\, d\Gamma_b = -\gamma h \frac{\partial z}{\partial x} dx \tag{6}$$

4. by using a first order Taylor expansion, all the differences $[\cdot]_{x_1}^{x_2}$ become differential expressions.

On the whole, in the limit as dx approaches zero, Eqs. (4) and (5) become:

$$\frac{\partial h}{\partial t} + \frac{\partial}{\partial x}(uh) = 0$$
$$\frac{\partial}{\partial t}(\rho uh) + \frac{\partial}{\partial x}\left(\rho u^2 h + \gamma\frac{h^2}{2}\right) = -\gamma h\frac{\partial z}{\partial x}$$

Considering the bed elevation as a variable of the problem and introducing the constraint that the bed cannot move, i.e. $\partial z/\partial t = 0$, the system becomes:

$$\frac{\partial}{\partial t}\mathbf{U} + \frac{\partial}{\partial x}\mathbf{F}(\mathbf{U}) + \mathbf{H}\frac{\partial \mathbf{U}}{\partial x} = 0 \tag{7}$$

where

$$\mathbf{U} = \begin{bmatrix} h \\ uh \\ z \end{bmatrix}; \quad \mathbf{F} = \begin{bmatrix} uh \\ u^2 h + \frac{1}{2} g h^2 \\ 0 \end{bmatrix}; \quad \mathbf{H} = \begin{bmatrix} 0 & 0 & 0 \\ 0 & 0 & gh \\ 0 & 0 & 0 \end{bmatrix} \tag{8}$$

With this approach, the system is clearly *nonconservative* due to the presence of the term $\mathbf{H}\partial\mathbf{U}/\partial x$, where $\mathbf{H}$ is the matrix of the *nonconservative fluxes*. Therefore, the vector $\mathbf{U}$ is no longer the vector of conserved variables, but we will keep on calling it such, meaning that its components come directly from the formulation of conservation principles.

2.2.1. Eigenstructure analysis of the extended SW system

In the following we briefly present the eigenstructure analysis of system (7) in terms of conserved variables. For a detailed analysis we address the reader to [22, Chapter 3], while in Appendix A a detailed analysis in term of primitive variables is given.

Considering the Jacobian matrix of the conservative fluxes $\mathbf{J_U} = d\mathbf{F}/d\mathbf{U}$, Eq. (7) can be written in the following quasi-linear form:

$$\frac{\partial \mathbf{U}}{\partial t} + \mathbf{A}\frac{\partial \mathbf{U}}{\partial x} = 0 \tag{9}$$

where $\mathbf{A} = \mathbf{J_U} + \mathbf{H}$. The relevant eigenvalues λ_i that satisfy the relation

$$\det|\mathbf{A} - \lambda_i \mathbf{I}| = 0 \tag{10}$$

are:

$$\lambda_1 = u - \sqrt{gh}; \quad \lambda_2 = 0; \quad \lambda_3 = u + \sqrt{gh} \tag{11}$$

The corresponding right eigenvectors, satisfying the relation

$$\mathbf{A}\mathbf{R}^i = \lambda_i \mathbf{R}^i$$

are:

$$\mathbf{R}^1 = \begin{bmatrix} 1 \\ u - \sqrt{gh} \\ 0 \end{bmatrix}; \quad \mathbf{R}^2 = \begin{bmatrix} 1 \\ 0 \\ (u^2/gh - 1) \end{bmatrix}; \quad \mathbf{R}^3 = \begin{bmatrix} 1 \\ u + \sqrt{gh} \\ 0 \end{bmatrix} \tag{12}$$

It can be noticed that the 1st and the 3rd characteristic fields are equivalent to the classical SW PDE system over a flat-bed; therefore (see e.g. [12]) they are genuinely non-linear and can develop either shock or rarefaction waves. Focusing on the 2nd characteristic field, since $\lambda_2 = 0$, we have:

$$\nabla\lambda_2(\mathbf{U}) \cdot \mathbf{R}^2(\mathbf{U}) = 0 \quad \forall \mathbf{U} \in \mathbb{R}^n \tag{13}$$

This field is therefore linearly degenerate and the relevant waves are contact waves.

In case of conservative systems, it is well-known that across a contact wave both the Rankine–Hugoniot (RH) relations and the Riemann Invariants (RIs) hold. As we will show further, this might be no longer true in case of nonconservative systems. In order to prove the peculiar features of the contact waves in nonconservative systems, we need to obtain the shock relations valid across a bed step.

2.3. Shock relations and the Generalized Rankine–Hugoniot equations

The relations valid across a discontinuity in the flow variables can be obtained from Eqs. (4) and (5) by using the following two assumptions:

(a) The control volume is infinitesimal (see [21, Chapter 10]).
(b) The control volume moves with velocity u_0 equal to the shock speed S. Therefore, $u_r = u - S$.

Let us consider a generic function $\psi(x,t)$ that represents $h(x,t)$ in (4) and the product $u(x,t)h(x,t)$ in (5). The consequences of these assumptions are the following:

1. referring to Fig. 2, inside the infinitesimal control volume of length δx the continuous variations of $\psi(x,t)$ can be disregarded because they are infinitesimal of higher order with respect to the discontinuous variations. Therefore, in a small interval around the discontinuity, the function can be considered as piecewise constant;
2. let us call ψ_L, ψ_R the values of the function $\psi(x,t)$ on the left and on the right of the discontinuity, respectively. If the control volume moves with a velocity equal to the shock speed, i.e. $v_{cv}|_{x_1(t)} = v_{cv}|_{x_2(t)} = S$, the value of the integral is constant because both the argument and the length of the integration interval do not change in time, so we obtain

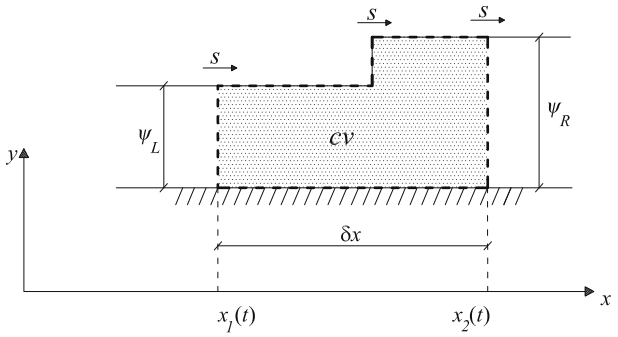

Fig. 2. Control volume used to derive the Rankine–Hugoniot relation.

$$\frac{d}{dt}\int_{x_1(t)}^{x_2(t)} \psi(x,t)dx = 0 \tag{14}$$

Therefore, the time derivatives of the integral terms in (4) and (5) become null.

It is now possible to write the specific shock relations valid for flat-bed and for discontinuous-bed.

2.3.1. The flat-bed case

In case of flat-bed, considering the previous results, Eq. (4) becomes:

$$[hu_r]_{x_1(t)}^{x_2(t)} = h_R(u_R - S) - h_L(u_L - S) = 0$$

where the subscripts L, R indicate the values of the functions, respectively on the left and on the right of the discontinuity. This equation can be rewritten as:

$$h_R u_R - h_L u_L = S(h_R - h_L) \tag{15}$$

Similarly Eq. (5) becomes:

$$\rho[hu v_r]_{x_1(t)}^{x_2(t)} = P_1 - P_2$$

$$h_R u_R(u_R - S) - h_L u_L(u_L - S) = g\frac{h_L^2}{2} - g\frac{h_R^2}{2}$$

so we finally obtain:

$$\left(u_R^2 h_R + g\frac{h_R^2}{2}\right) - \left(u_L^2 h_L + g\frac{h_L^2}{2}\right) = S(h_R u_R - h_L u_L) \tag{16}$$

Both equations can be written in the standard RH vectorial form:

$$\mathbf{F}_R - \mathbf{F}_L = S(\mathbf{U}_R - \mathbf{U}_L) \tag{17}$$

where $\mathbf{F}, \mathbf{U}$ are given by (8).

Given a left state $\mathbf{U}_L$, the set of all the states $\mathbf{U}_R$ which satisfy the previous equation gives a curve in the state space called Hugoniot Locus (HL).

It is possible now to understand how the shock theory approximates the real world in case of a flat-bed. Let us consider an hydraulic jump with a well-defined roller, moving with speed S, and a control volume moving with the same velocity, bounded by two vertical sections positioned sufficiently far from the turbulent vortex, such that along these sections the SW approximations hold. Thus, conservation of mass and momentum written for this control volume leads to an expression equivalent to Eq. (17). It is interesting to notice that inside this control volume the flow field does not satisfy the SW assumptions at all. However, due to the stationarity of the formulation (see Eq. (14)), the result is independent both from what happens inside the control volume and from its length. Therefore, we can conclude that the shock theory describes quite well an hydraulic jump with a roller but reduces it to a pointwise discontinuity (see e.g. [13], sect. 11.6). This is actually consistent with the SW assumption that water depth is much smaller than the typical horizontal scale. Considering that the length of a hydraulic jump is proportional to the water depth [8], it is clear that its length can be considered negligible. In this view, it is also possible to justify why an inviscid fluid dissipates energy across a shock. All the viscid (and turbulent) dissipations are actually hidden in the discontinuity that represents what in reality is a highly dissipative turbulent vortex. When a hydraulic jump does not present a well-defined roller, shock theory does not describe the actual behavior of the flow so well because the SW conditions are not matched on the boundaries of the control volume.

2.3.2. The discontinuous bed case

We look now for a relation valid across a bed discontinuity. From a mathematical point of view, the approach is exactly the same as that used in the previous case, but now the shock speed is null, i.e. $S = 0,\ u_r = u$ and x_1, x_2 are no longer functions of time. Eq. (4) becomes:

$$h_R u_R - h_L u_L = 0 \tag{18}$$

and expresses the conservation of the discharge. Eq. (5) needs some attention. Referring to Fig. 3 we can write [17,4]:

$$[(hu)u_r]_{x_1}^{x_2} = \frac{P_1}{\rho} - \frac{P_2}{\rho} + \int_{\Gamma_b(x_1(t))}^{\Gamma_b(x_2(t))} \frac{p_{bx}}{\rho}\, d\Gamma_b \tag{19}$$

The left-hand terms become:

$$[(hu)\,v_r]x_1^{x_2} = h_R u_R^2 - h_L u_L^2.$$

The last term on the right-hand side represents the x-component of the integral pressure exerted by the bottom along Γ_b. Along the discontinuity, Γ_b becomes a function of the y-coordinate. Indicating with z_L and z_R the elevations to the left and right sides (respectively) of the bottom discontinuity, the integral of the bottom pressure (thrust term) can be written as:

$$D = \int_{\Gamma_b(x_1)}^{\Gamma_b(x_2)} \frac{p_{bx}}{\rho} d\Gamma_b = \int_{z_L}^{z_R} \frac{p_{bx}}{\rho} dy \tag{20}$$

It is clear that the pressure distribution must depend on the actual flow behavior in the neighborhood of the bed discontinuity, including the presence of a dissipative vortex near the step and the non-hydrostatic features of the flow field. Moreover, we must keep in mind that in our approach, deriving from shock theory, all the non-SW flow region is lumped in a single discontinuity, because of its limited width. Lacking experimental evidence and reliable solutions (even approximated) of the fully vertical 2D Reynold equations able to lead to a trustworthy pressure distribution, some hypotheses must be introduced. Nonetheless it must be stressed that any assumption regarding pressure actually conceals an assumption on the dissipation magnitude and on the non-hydrostaticity. Last but not least, unlike what happens in the flat-bed case, because of the presence of the thrust term, the relation connecting the flow variables before and after the step is not independent from what happens *inside* the control volume.

In this paper we will use the following relation, proposed by [17] (used also in [4,18]) on the basis of physical considerations:

$$D = -g\left(h_k - \frac{|z_R - z_L|}{2}\right)(z_R - z_L) \quad \text{with} \quad k = \begin{cases} L & \text{if } z_L \leqslant z_R \\ R & \text{otherwise} \end{cases} \tag{21}$$

Eq. (21) derives from an hydrostatic distribution that depends on the water depth on the lower side of the step. Note that this expression is exact for static conditions and converges to the differential expression (6) in the case of infinitesimal discontinuity. It is important to keep in mind that this expression constitutes an assumption valid in a wide range of flow conditions, but not for all: its validity decreases as $h_k/|tz_R - z_L|$ approaches unity and clearly ceases when $h_k < |z_R - z_L|$. Laboratory experiments are required to assess the physical soundness of Eq. (21) and find suitable expressions for flow conditions for which it is not applicable. In any case, the theoretical approach that has been followed in this work is generally valid and does not depend on the specific choice of this relation, whereas the results depend to some extent on it. This will be shown more clearly later in the paper.

Then, Eq. (19) can be written in the following form:

$$\left(h_R u_R^2 + g\frac{h_R^2}{2}\right) - \left(h_L u_L^2 + g\frac{h_L^2}{2}\right) = D \tag{22}$$

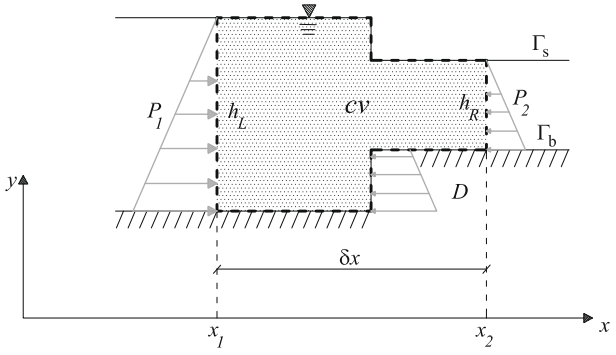

Fig. 3. Control volume used to obtain the Generalized Rankine–Hugoniot relations in case of discontinuous solution over the bed step.

Therefore, we can write Eq. (22) together with Eq. (18) in the following vectorial form:

$$\mathbf{F}_R - \mathbf{F}_L = \mathbf{D} \tag{23}$$

where $\mathbf{D}^T = (0, D, 0)$. This is a special case of the Generalized Rankine–Hugoniot (GRH) relation:

$$\mathbf{F}_R - \mathbf{F}_L = \mathbf{D} + S(\mathbf{U}_R - \mathbf{U}_L) \tag{24}$$

that can be obtained (see [18]) in the case of a fully mobile-bed. The origin of the extra term with respect to the standard RH relations lies in the nonconservative nature of the pressure term. It should be noticed that this relation can be obtained from the differential formulation by using the distribution theory (see e.g. [23,15,16]). Nevertheless, such an approach is not able to give a clear physical meaning to the extra term while using our approach this comes out straightforwardly.

Finally, as for the flat-bed case, given a left state $\mathbf{U}_L$ and a step with height $|z_R - z_L|$, the set of the right statesthat satisfy (24) defines a curve in the state space that will be called here Generalized Hugoniot–Locus (GHL).

3. Contact waves in nonconservative systems

In this section we will demonstrate that contact waves in nonconservative systems show features rather different with respect to fully conservative systems (Section 3.5). This result will be applied to the specific case of the contact wave that develops over a bed step (Section 3.6). In order to achieve this goal, for the sake of clarity, it is necessary to briefly recall some basic concepts relative to contact waves. This is done in Sections 3.2, 3.3 and 3.4 where we followed [20]. For a comprehensive analysis of the problem for conservative systems we also refer the reader to [13].

3.1. Conservative vs. nonconservative systems

A generic conservative hyperbolic system can be written in the following way:

$$\frac{\partial \mathbf{U}}{\partial t} + \frac{\partial \mathbf{F}}{\partial x} = 0 \tag{25}$$

where $\mathbf{U}$ is the vector of the conservative variables and $\mathbf{F}$ is the vector of the conservative fluxes. The relevant eigenvalues λ_i are defined by:

$$\det|\mathbf{J}_\mathbf{U} - \lambda_i \mathbf{I}| = 0$$

where $\mathbf{J}_\mathbf{U}$ is the Jacobian matrix $d\mathbf{F}/d\mathbf{U}$, while the right eigenvectors satisfy the following relation:

$$\mathbf{J}_\mathbf{U}\mathbf{R}^k - \lambda_k \mathbf{R}^k = 0 \tag{26}$$

Discontinuous solutions of (25) satisfy the RH relations, namely Eq. (17).

A generic nonconservative hyperbolic problem can be written in the following way:

$$\frac{\partial \mathbf{U}}{\partial t} + \frac{\partial \mathbf{F}}{\partial x} + \mathbf{H}\frac{\partial \mathbf{U}}{\partial x} = 0 \tag{27}$$

where $\mathbf{U}$ is the vector of the conserved variables, $\mathbf{F}$ is the vector of the conservative fluxes, while $\mathbf{H}$ is the matrix of the nonconservative fluxes. Eq. (27) can be written in the following quasi-linear form:

$$\frac{\partial \mathbf{U}}{\partial t} + \mathbf{A}\frac{\partial \mathbf{U}}{\partial x} = 0 \tag{28}$$

where $\mathbf{A} = \mathbf{J}_\mathbf{U} + \mathbf{H}$ and $\mathbf{J}_\mathbf{U} = d\mathbf{F}/d\mathbf{U}$. The relevant eigenvalues λ_i are defined by:

$$\det|\mathbf{A} - \lambda_i \mathbf{I}| = 0 \tag{29}$$

while the corresponding right eigenvectors satisfy the relation:

$$\mathbf{A}\mathbf{R}^i = \lambda_i \mathbf{R}^i$$

or equivalently:

$$\mathbf{J}_\mathbf{U}\mathbf{R}^i - \lambda_i \mathbf{R}^i = -\mathbf{H}\mathbf{R}^i \tag{30}$$

Discontinuous solutions of (27) satisfy the GRH relations, namely Eq. (24).

3.2. Integral curves and riemann invariants

Given an hyperbolic system, either conservative or nonconservative, composed by n differential equations in the variables $\mathbf{U} = (U_1, \ldots, U_n)$, let us consider the generic eigenvalue λ_k and the relevant right eigenvector $\mathbf{R}^k(\mathbf{U})$. In the phase-space, i.e. in the n-dimensional space of the variables, $\mathbf{R}^k(\mathbf{U})$ can be considered as a vector field, i.e. a function $\mathbb{R}^n \to \mathbb{R}^n$. As for every vector field, we can consider the lines everywhere tangent to $\mathbf{R}^k(\mathbf{U})$ (a concept analogous to the streamlines for the velocity field).

Such lines are called Integral Curves (ICs) associated with $\mathbf{R}^k(\mathbf{U})$, and can be expressed, as any other curve, in parametric form, i.e. as a function of a generic parameter $\xi \in \mathbb{R}$:

$$\mathbf{s}^k = s^k(\xi) = \begin{bmatrix} U_1(\xi) \\ \vdots \\ U_n(\xi) \end{bmatrix} \tag{31}$$

Since the vector tangent to a curve is obtained from the derivative of the curve with respect to the parameter ξ, the condition of parallelism between the tangent vector and the vector field can be expressed as

$$\frac{d}{d\xi}\mathbf{s}^k = \alpha(\xi)\mathbf{R}^k \tag{32}$$

where $\alpha(\xi)$ is a scaling factor that depends on the particular parametrization of the curve. Without loss of generality, we can set $\alpha(\xi) \equiv 1$.

It is possible to obtain the IC curve simply by integration of the previous system in which the dependency of $\mathbf{R}^k(\mathbf{U})$ on ξ is considered through $\mathbf{U}(\xi)$. Alternatively, it is possible to get an expression directly in terms of $\mathbf{U}$. In fact, Eq. (32) can be rewritten in the following form:

$$\frac{dU_i}{R_i^k} = d\xi, \quad i = 1, \ldots, n \tag{33}$$

where R_i^k is the ith component of $\mathbf{R}^k$. Noting that the terms on the right-hand side in Eqs. (33) are all equal, the dependency on ξ can be removed, giving the following set of equations:

$$\frac{dU_1}{R_1^k} = \frac{dU_2}{R_2^k} = \cdots = \frac{dU_n}{R_n^k} \tag{34}$$

where only $n-1$ equations are linearly independent.

A k-Riemann invariant is defined as a surface $w(\mathbf{U}) : \mathbb{R}^n \rightarrow \mathbb{R}$ such that its gradient is orthogonal to the kth eigenvector:

$$\nabla w(\mathbf{U}) \cdot \mathbf{R}^k = 0 \quad \forall \mathbf{U} \in \mathbb{R}^n \tag{35}$$

There are three main properties of these surfaces:

1. A k-Riemann invariant $w(\mathbf{U})$ is constant along the integral curve $\mathbf{s}^k(\xi)$. In fact, the variation of $w(\mathbf{U})$ along the curve $\mathbf{s}^k(\xi)$ is given by:

$$\frac{d}{d\xi} w(\mathbf{s}^k(\xi)) = \nabla w \cdot \frac{d}{d\xi}\mathbf{s}^k(\xi) \tag{36}$$

   Using Eq. (32) with $\alpha(\xi) \equiv 1$ and Eq. (35), we obtain:

$$\frac{d}{d\xi} w(\mathbf{s}^k(\xi)) = \nabla w \cdot \mathbf{R}^k = 0 \tag{37}$$

   In other words, the integral curve belongs to the level set of the given k-Riemann invariant;
2. there exist $n-1$ linearly independent k-Riemann invariants associated with the k-th eigenvector;
3. given a point $\mathbf{U}_0$, the intersection of the $n-1$ level sets $w^i(\mathbf{U}) = const$, with $i = 1, \ldots, n-1$, passing through $\mathbf{U}_0$, is equivalent to the integral curve $\mathbf{s}^k(\xi)$ passing through $\mathbf{U}_0$.

Thanks to this last property, the $n-1k$-Riemann invariants can be computed by means of Eq. (34) instead of using the definition (35).

3.3. Linearly degenerate fields

The characteristic field associated with the kth eigenvalue is said to be linearly degenerate when:

$$\nabla \lambda_k(\mathbf{U}) \cdot \mathbf{R}^k(\mathbf{U}) = 0 \quad \forall \mathbf{U} \in \mathbb{R}^n \tag{38}$$

This means that, thanks to (35), $\lambda_k(\mathbf{U})$ is a k-Riemann invariant. From (37) follows:

$$\frac{d}{d\xi} \lambda_k(\mathbf{s}^k(\xi)) = 0 \quad \forall \xi \in \mathbb{R} \tag{39}$$

Therefore, the eigenvalue remains constant along the integral curve. As a particular case, when the eigenvalue λ_k does not depend on $\mathbf{U}$, it is not only constant along the integral curve but all over the state space.

The type of wave associated with a linearly degenerate field is called a contact wave or contact discontinuity. The properties of such waves will be discussed in the following two sections.

3.4. Properties of contact waves in conservative systems

Let λ_k be an eigenvalue whose characteristic field is linearly degenerate and let $\mathbf{U}_L$ be a generic state. It can be proven that the associated contact wave is described by a discontinuous function of the type:

$$\mathbf{U}(x,t) = \begin{cases} \mathbf{U}_L & x < t\lambda_k \\ \mathbf{U}(\xi) & x > t\lambda_k \end{cases} \tag{40}$$

i.e., by a function $\mathbf{U}(x,t)$ characterized by a discontinuity moving with constant speed λ_k, where $\mathbf{U}(\xi)$ is any state connected to $\mathbf{U}_L$ by means of the relevant k-Riemann invariants. In other words, $\mathbf{U}(\xi)$ must lie on the IC passing through $\mathbf{U}_L$:

$$\frac{d}{d\xi}\mathbf{U}(\xi) = R^k, \quad \mathbf{U}(0) = \mathbf{U}_L \tag{41}$$

The proof is as follows (see [20, Chapter 17]). Eq. (40) is a discontinuous solution of the system (25) only if it satisfies the relevant RH condition:

$$[\mathbf{F}] = S[\mathbf{U}] \tag{42}$$

where $[\cdot]$ indicates the jump in the quantity inside the brackets across the discontinuity moving with speed S. Therefore, in order to prove the thesis, we must verify that the previous equation holds when evaluated between $\mathbf{U}_L$ and $\mathbf{U}(\xi)$ and with $S = \lambda_k$:

$$[\mathbf{F} - S\mathbf{U}]_0^{\xi} = 0.$$

If ξ is infinitesimal, the previous condition can be rewritten in the following equivalent differential form:

$$\frac{d}{d\xi}(\mathbf{F} - S\mathbf{U}) = 0.$$

The derivative can be expanded in the following way:

$$\frac{d}{d\xi}(\mathbf{F} - S\mathbf{U}) = \frac{d\mathbf{F}}{d\mathbf{U}}\frac{d}{d\xi}\mathbf{U}(\xi) - S\frac{d}{d\xi}\mathbf{U}(\xi) \tag{43}$$

Considering Eq. (41), recalling that $d\mathbf{F}/d\mathbf{U} = \mathbf{J}_\mathbf{U}$, and finally using Eq. (26), we obtain:

$$\frac{d}{d\xi}(\mathbf{F} - S\mathbf{U}) = \mathbf{J}_\mathbf{U}\mathbf{R}^k - \lambda_k\mathbf{R}^k = 0$$

Hence, the pair $(\mathbf{U}_L, \mathbf{U}(\xi))$ satisfies the RH condition with $S = \lambda_k$, and so Eq. (40) is actually a discontinuous solution of (25). It should be noticed that since $\mathbf{U}(\xi)$ satisfies the RH relations, it must lie on the HL. Noting that $\mathbf{U}(\xi)$ also lies on the IC, we can conclude that the HL curves and the IC curves coincide in case of contact waves in conservative systems. In other words, both Riemann invariants and RH relations hold at the same time.

3.5. Properties of contact waves in nonconservative systems

In nonconservative systems, discontinuous solutions must satisfy the GRH relation (see Eq. 24) which is characterized by the nonconservative term $\mathbf{D}$. This generates some differences in the features of contact waves with respect to conservative systems.

Theorem 1. *Given a generic nonconservative system of type (27) and a generic reference state $\mathbf{U}_L$, if the kth characteristic field relative to the eigenvalue λ_k is linearly degenerate, then the associated contact wave is described by a discontinuous function of type*

$$\mathbf{U}(x,t) = \begin{cases} \mathbf{U}_L & x < t\lambda_k \\ \mathbf{U}(\xi) & x > t\lambda_k \end{cases} \tag{44}$$

where $\mathbf{U}(\xi)$ is any state connected to $\mathbf{U}_L = \mathbf{U}(0)$ by means of the relevant k-Riemann invariants, if the following equation holds:

$$-\int_0^{\xi} \mathbf{H}\mathbf{R}^k d\xi = \mathbf{D} \tag{45}$$

Proof. Function (44) is a discontinuous solution of (27) if it satisfies the GRH condition (24) that, for the specific case, becomes:

$$[\mathbf{F} - S\mathbf{U}]_0^{\xi} - \mathbf{D} = 0 \tag{46}$$

Here $[\cdot]_0^{\xi}$ indicates the variation of the function inside the brackets evaluated in two points (0 and ξ) of the same IC. If ξ is infinitesimal, the previous variation can be rewritten as a differential expression:

$$\frac{d}{d\xi}(\mathbf{F} - S\mathbf{U} - \mathbf{D}) = 0 \tag{47}$$

Let us set $S = \lambda_k$ and expand the derivatives:

$$\frac{d}{d\xi}(\mathbf{F} - S\mathbf{U} - \mathbf{D}) = \frac{d\mathbf{F}}{d\mathbf{U}}\frac{d}{d\xi}\mathbf{U}(\xi) - \lambda_k \frac{d}{d\xi}\mathbf{U}(\xi) - \frac{d\mathbf{D}}{d\xi} \tag{48}$$

Using $d\mathbf{F}/d\mathbf{U} = \mathbf{J_U}$ and relation (41) we obtain:

$$\frac{d}{d\xi}(\mathbf{F} - S\mathbf{U} - \mathbf{D}) = \mathbf{J_U}\mathbf{R}^k - \lambda_k \mathbf{R}^k - \frac{d\mathbf{D}}{d\xi} \tag{49}$$

By using Eq. (30) we get:

$$\frac{d}{d\xi}(\mathbf{F} - S\mathbf{U} - \mathbf{D}) = -\mathbf{H}\mathbf{R}^k - \frac{d\mathbf{D}}{d\xi} \tag{50}$$

In order to obtain (47) we must set:

$$-\mathbf{H}\mathbf{R}^k - \frac{d\mathbf{D}}{d\xi} = 0 \tag{51}$$

which, integrating between states L and ξ, gives (45). □

Analogously to the conservative case, under condition (45) IC coincides with the GHL. Moreover, in nonconservative systems with a linearly degenerate field, Eq. (45) could be used to evaluate $\mathbf{D}$ without resorting to the direct derivation of the GRH relation, which could present several difficulties.

As already noticed, in our specific case the eigenvalue λ_k does not depend on $\mathbf{U}$ ($\lambda_2 = 0$, see Eq. (11)). In this particular case, the following theorem holds:

Theorem 2. *Given a nonconservative system of type (27) and a generic reference state $\mathbf{U}_L$, if the kth characteristic field associated with the eigenvalue λ_k is linearly degenerate and does not depend on $\mathbf{U}$, then the associated contact wave is described by a discontinuous function of type*

$$\mathbf{U}(x,t) = \begin{cases} \mathbf{U}_L & x < t\lambda_k \\ \mathbf{U}(\epsilon) & x > t\lambda_k \end{cases} \tag{52}$$

where $\mathbf{U}(\epsilon)$ is any state connected to $\mathbf{U}_L = \mathbf{U}(0)$ by means of the GRH relation.

Proof. Unlike the previous cases, we are not bound to choose the right status of the wave along the IC to be guaranteed that λ_k is constant because the eigenvalue does not depend on $\mathbf{U}$. Therefore, if $\mathbf{U}(\epsilon)$ belongs to the GHL, then (40) is a discontinuous solution of (27). □

Corollary 1. *In contact waves of nonconservative systems where the relevant eigenvalue does not depend on $\mathbf{U}$, IC and GHL may not coincide.*

Proof. We have seen that IC and GHL coincide if Eq. (45) holds. This may not happen because the hypotheses used to obtain $\mathbf{D}$ in the GRH relation are not the same as those used to obtain the partial differential equation system (and indirectly, to obtain the terms appearing on the left of the relation). Therefore, condition (45) must be checked for any specific problem: if it is not verified, IC and GHL do not coincide. □

As reported in Appendix B, all the theory developed above in terms of conserved variables can be easily reformulated in terms of primitive variables.

3.6. Contact waves in the step SW problem

We have already shown in Section 2.2.1 that the SW problem with a bed step presents a linearly degenerate field associated with $\lambda_2 = 0$. The analysis of the peculiar features of the associated contact waves will be performed using the physical variables $\mathbf{W}^T = (h, u, z)$ instead of the conserved variables $\mathbf{U}^T = (h, uh, z)$, to make its derivation is more straightforward and clear.

What we want to show is that, assuming that $\mathbf{D}$ is given by (21), IC does not coincide with GHL. Mathematically, in terms of primitive variables this means that (see Appendix B):

$$-\int_0^{\xi} \mathbf{H}\mathbf{B}\widetilde{\mathbf{R}}^2 d\xi \neq \mathbf{D}$$

where $\mathbf{B}$ and $\widetilde{\mathbf{R}}^2$ are defined in Appendix B.

The left-hand side term can be evaluated by using the parametric expression of the IC curve passing through a generic state $\mathbf{W}_L^T = (h_L, u_L, z_L)$, i.e. Eq. (76):

$$-\int_0^{\hat{\xi}} \mathbf{HB}\widetilde{\mathbf{R}}^2 d\xi = -\int_0^{\hat{\xi}} \begin{bmatrix} 0 \\ u^2(\xi) - gh(\xi) \\ 0 \end{bmatrix} d\xi$$

It can be noticed that only the second equation, the one relevant to the momentum equation, is not null.

Setting $\hat{\xi} = h_R - h_L$ and $u(\hat{\xi}) = u_R$, after some manipulations one gets:

$$-\int_0^{h_R - h_L} \left(\left(\frac{h_L u_L}{\xi + h_L} \right)^2 - g(h_L + \xi) \right) d\xi = \left(\frac{1}{2} g h_R^2 + u_R^2 h_R \right) - \left(\frac{1}{2} g h_L^2 + h_L u_L^2 \right) \tag{53}$$

As far as the $\mathbf{D}$ term is concerned, the only component which is not null is the second. Setting $z_R(\hat{\xi}) = z_R$, from (76) follows, after some manipulations:

$$z_R - z_L = (h_L - h_R) + \left(\frac{u_L^2}{2g} - \frac{u_R^2}{2g} \right) \tag{54}$$

Substituting in (21) one gets

$$D = -g\left(h_k - \frac{1}{2} \left| (h_L - h_R) + \left(\frac{u_L^2}{2g} - \frac{u_R^2}{2g} \right) \right| \right) \left((h_L - h_R) + \left(\frac{u_L^2}{2g} - \frac{u_R^2}{2g} \right) \right)$$

which is clearly different from (53). The difference between IC and GHL is presented also graphically in Fig. 4 where the two curves passing through the point $\mathbf{W}_L^T = (5, 2, 0)$ are plotted. The detailed expression of the parametric form of the GHL curve is given in the subsequent section.

We can conclude that, for the present problem, the standing wave that forms over a bed step is a special contact discontinuity that, unlike standard contact waves in conservative systems, is not characterized by the constancy of the Riemann Invariants (which would imply both mass and energy conservation, see Appendix A), but by the GRH conditions, which implies that mass and momentum are conserved. This result answers to one of the basic question raised in this paper: the nature of the wave that develops over the step and its properties. Such a wave is actually a contact wave but, because of the nonconservative nature of the relevant PDE system, Riemann invariants are not constant across it. Therefore, the apparent contradiction between the mathematical and the physical approaches, present so far in the literature, is definitely resolved.

Nevertheless, the use of GRH relations to characterize the contact wave leads to a significant drawback: these relations may give multiple solutions. Therefore, some constraints must be introduced to rule out the non physical solutions: in the case of a genuinely non-linear shock, the constraint derives from the entropy condition $\lambda(\mathbf{U}_L) > \lambda(\mathbf{U}_R)$. It is clear that this constraint does not hold in the contact wave shock because the eigenvalue is constant both upstream and downstream of the discontinuity. It is therefore necessary to introduce some other constraints. This topic is developed in detail in the following section.

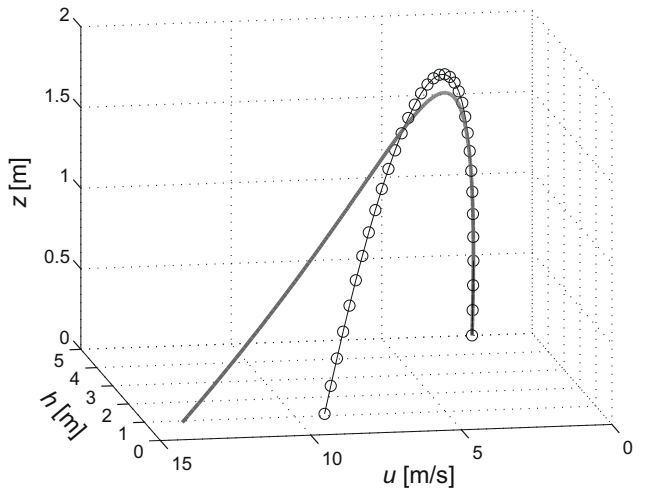

Fig. 4. Comparison between the Generalized Hugoniot–Locus (thick solid line) and the integral curve starting from $\mathbf{W}_L = (5, 2, 0)$.

4. Characterization of the step GHL

Given a left state $\mathbf{W}_L$, the step GHL curve represents the set of all the states $\mathbf{W}(\xi)$ that can be connected through a step contact wave to $\mathbf{W}_L$. In the following, we will distinguish whether a point (state) of the curve is *possible* from a mathematical point of view (i.e. simply a solution of the equation that defines the GHL curve), or is *admissible* from a physical point of view (i.e., it also satisfies the constraints that will be defined later). As will be shown, from the analysis of the plot representing the GHL curve it is straightforward to determine which parts of the curve are admissible and which are simply possible.

4.1. The parametric form of the GHL

The parametric form of the GHL can be obtained starting from a parametrization of the water depth as a function of ξ, i.e. $h(\xi) = h_L + \xi$. The other components of the GHL curve can be obtained from Eqs. (18) and (22), i.e., by imposing the conservation of the discharge and of the momentum across the bed discontinuity. The resulting expression is similar to the parametric form of the IC curve (Eq. (76) and Appendix A): in this case, the third component $z(\xi)$ is evaluated by using the equation of energy conservation instead of momentum conservation. Without loss of generality we can set $z_L = 0$. The curve then becomes:

$$\mathbf{s}^{\pm}_{GHL}(\xi) = \begin{bmatrix} h(\xi) = h_L + \xi \\ u(\xi) = \frac{h_L u_L}{\xi + h_L} \\ z^{\pm}(\xi) = \begin{cases} h_L \pm \frac{1}{\sqrt{g}} \sqrt{-2h_L u_L^2 + 2h(\xi)u^2(\xi) + gh^2(\xi)} \\ -h(\xi) \pm \frac{1}{\sqrt{g}} \sqrt{2h_L u_L^2 - 2h(\xi)u^2(\xi) + gh_L^2} \end{cases} \end{bmatrix} \tag{55}$$

where $z^+(\xi)$ corresponds to a positive step ($z_R > z_L = 0$) and $z^-(\xi)$ to a negative step ($z_R < z_L = 0$). Notice that the limits of validity of (21) require that the height of the step, must be smaller than h_L for a positive step and than $h(\xi)$ for a negative step. Mathematically this becomes:

$$z^+(\xi) - h_L < 0$$
$$z^-(\xi) + h(\varepsilon) > 0$$

Therefore, the expressions of $z^{\pm}(\xi)$ in Eq. (55) become:

$$z^{\pm}(\xi) = \begin{cases} h_L - \frac{1}{\sqrt{g}} \sqrt{-2h_L u_L^2 + 2h(\xi)u^2(\xi) + gh^2(\xi)} \\ -h(\xi) + \frac{1}{\sqrt{g}} \sqrt{2h_L u_L^2 - 2h(\xi)u^2(\xi) + gh_L^2} \end{cases}$$

In the following sections we will analyze the features of the GHL curves, considering separately the cases of positive and negative.

4.2. Positive step

Fig. 5(a) shows the $\mathbf{s}^+_{GHL}$ curves starting from $\mathbf{W}_L$ points characterized by a fixed value of $h_L = 2$ m and for values of u_L ranging from 0 to 4.43 m/s, which corresponds to Froude numbers ranging from 0 to 1. Fig. 5b shows the $\mathbf{s}^+_{GHL}$ curves starting from $\mathbf{W}_L$ points with a fixed value of $h_L = 2$ m and values of u_L greater than 4.43 m/s, which corresponds to Froude numbers greater than 1. In both figures, the starting points $\mathbf{W}_L$ are connected by a magenta bold line. We recall that the $\mathbf{s}^+_{GHL}$ curves represent the *possible* points, i.e. states to which $\mathbf{W}_L$ can be connected through a step contact wave, in the case of positive step. In particular, the line starting from point $\mathbf{W}_L = \mathbf{A}$ and ending at point $\mathbf{W}(\xi) = \mathbf{B}$ is highlighted: this line will be considered later in this paragraph to explain some features of the GHLs.

What can be inferred from the analysis of the curves is that:

1. Each curve has a maximum, and the Froude number in that point is equal to 1. In fact, deriving $z^+(\xi)$ with respect to ξ one obtains:

$$\frac{\partial}{\partial \xi} z^+(\xi) = -\frac{1}{\sqrt{g}} \frac{g(\xi + h_L) - \frac{h_L^2 u_L^2}{(\xi + h_L)^2}}{\sqrt{g(\xi + h_L)^2 - 2h_L u_L^2 + 2h_L^2 \frac{u_L^2}{\xi + h_L}}} \tag{56}$$

Let ξ_{cr} be the value of ξ for which $\partial z^+(\xi_{cr})/\partial \xi = 0$; at that point the numerator must be null:

$$g(\xi_{cr} + h_L) - \frac{h_L^2 u_L^2}{(\xi_{cr} + h_L)^2} = 0. \tag{57}$$

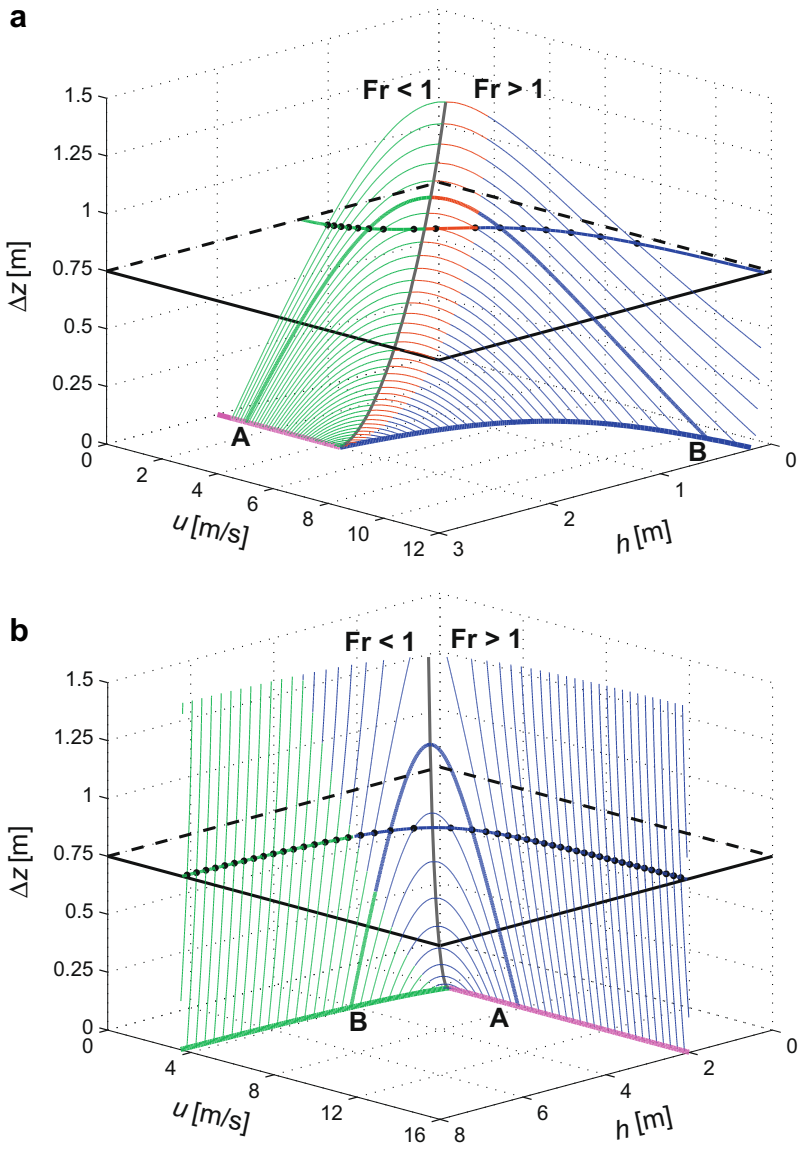

Fig. 5. $\mathbf{s}^{\pm}_{GHL}$ curves starting from $\mathbf{W}_L$ points (magenta line) with Froude numbers: (a) ranging from 0 to 1; (b) greater than 1. In green: admissible points; in blue: points ruled out by the energy principle; in red: points ruled out by the continuation principle (see text). For the meaning of points A and B, see text.

By using Eqs. (55), this relation can be rewritten as:

$$1 = \frac{(h_L u_L)^2}{g(\xi_{cr} + h_L)^3} = \frac{u^2(\xi_{cr})}{gh(\xi_{cr})} \tag{58}$$

which corresponds to the condition $Fr^2 = 1$.

2. Looking at Fig. 5(a), it is possible to individuate two branches in any GHL curve: the first, spanning from $\mathbf{W}_L$ to the maximum, presents possible right points in subcritical conditions, the second presents possible right states in supercritical conditions. Analogously, looking at Fig. 5(b), it is possible to identify the supercritical branch, spanning from $\mathbf{W}_L$ to the maximum, and the subcritical branch.
3. Considering the physical principle that a fluid particle can move only from condition with higher energy (E) to condition with lower energy, we can individuate admissible points $\mathbf{W}(\hat{\xi})$ where

$$E(\mathbf{W}_L) > E(\mathbf{W}(\hat{\xi})) \tag{59}$$

The pieces of the GHL curves that are made inadmissible by this constraint are plotted in blue. Looking at Fig. 5(a), the energy constraint rules out part of the supercritical branch of the GHL curves starting from subcritical $\mathbf{W}_L$. Note that the red parts of the supercritical branch remain admissible from an energetic point of view. On the other hand, considering the curves with supercritical starting points $\mathbf{W}_L$ (Fig. 5(b)), the energy constraint rules out the whole supercritical branch and the upper part of the subcritical one.

4. Let us consider the bold $\mathbf{s}^+_{GRL}$ curves going from points A to B, and a step with a generic height $\hat{z}_R$; the possible conditions over the step can be found by intersecting the $\mathbf{s}^+_{GRL}$ curve with a horizontal plane corresponding to $z = \hat{z}_R$. The following cases can be individuated:

$\hat{z}_R = 0$. This is the case with a null step (horizontal bed condition). The two states (points A and B) represent what in hydraulics is commonly defined as conjugate states of a hydraulic jump. If point $\mathbf{W}_L = \mathrm{A}$ is in supercritical conditions (Fig. 5(b)), admissible $\mathbf{W}(\xi)$ points can be either A (unchanged condition) or B (in subcritical conditions): this last case corresponds to a configuration of a steady shock over horizontal bed. In contrast, if point A is in subcritical conditions (Fig. 5(a)), point B is inadmissible: in fact, this represents an unentropic steady shock in which a subcritical left condition ($\mathbf{W}_L = \mathrm{A}$) is followed by a supercritical right condition ($\mathbf{W}(\xi) = \mathrm{B}$).

$\hat{z}_R > z^+(\xi_{cr})$. In this case there are no intersections between the plane $z = \hat{z}_R$ and the curve. This means that the status $\mathbf{W}_L$ is not able to develop a contact wave across the step. In other words, it is not possible to encounter a contact wave with a left value equal to that value of $\mathbf{W}_L$.

$0 < \hat{z}_R \leqslant z^+(\xi_{cr})$. In this case we can assume that the given height $\hat{z}_R$ is reached by a continuous increase in the step elevation from zero to $\hat{z}_R$. Consequently, the conditions over the step change continuously from the possible values at the zero level (points A or B in the plots) to the value at the level $\hat{z}_R$. As a consequence of this *Continuation Principle* (used in a similar way in [6]) it can be deduced that:

(a) If a point at zero level is admissible, we can continuously increase the step elevation from zero to $\hat{z}_R$, and $\mathbf{W}(\xi)$ at the level $\hat{z}_R$ will be admissible unless ruled out by the energy principle. As an example, in Fig. 5(a), point A corresponds to an admissible flow condition at zero level. Increasing the step height, we get admissible states (green line) up to the step level $\hat{z}_R$. Considering now Fig. 5(b), point B corresponds to admissible flow conditions at zero level. Increasing the step height, we obtain admissible states (green line) until a certain threshold level is reached, since for larger values of $\hat{z}_R$ the energy constraint is violated. In the same figure, point A corresponds to an admissible status as well. However, increasing the step height to any value $\hat{z}_R > 0$, the energy principles makes flow conditions inadmissible, and therefore the whole branch of the curve from A to the maximum, excluding the starting point, is inadmissible.

(b) If a point at zero level is inadmissible, we cannot start applying the continuation principle, and therefore it is impossible to reach *any* point of the relevant branch. We can conclude that the *whole* branch of a curve that starts from an inadmissible point at the zero level is inadmissible. As an example, in Fig. 5(a), point B is an inadmissible status at zero level, therefore the whole branch from B to the maximum is inadmissible, even though the part nearest to the critical status (plotted in red) would be allowed by the energy principle. From this reasoning we can argue that it is not possible to have a subcritical condition $\mathbf{W}_L$ on the left of the step and a supercritical condition on the right. The continuation principle herein introduced expresses, in an intuitive way, the *Monotonicity Criterion*, proved by [10], which states that any stationary discontinuity cannot cross the boundary of strict hyperbolicity.

5. In practical situations, the height of the step is fixed. In this case it is useful to have a graphic representation of the admissible states on the left and on the right of the given step. Let us consider the case with $\hat{z}_R = 0.75$ m. The set of the intersections of the $\mathbf{s}^+_{GHL}$ curves with the plane $z = \hat{z}_R$ (see Fig. 5(a) and (b) gives the lines that describe the conditions on the right side of the step. These lines are shown in the right plots of Fig. 6(a) and (b) for the subcritical and the supercritical case, respectively. The colors of the lines have the same meaning as the 3D case: in green, admissible states; in blue, states ruled out by the energy principle; in red, states ruled out by the continuation principle. In the left graphs the lines of the possible states on the left of the step are shown. The dashed lines represent inadmissible points because of the fact that the relevant $\mathbf{s}^+_{GHL}$ curves have no intersections with the given step, and therefore such left states $\mathbf{W}_L$ are not able to develop a contact wave across a step with $\hat{z}_R = 0.75$ m. It is useful to describe what happens to the contact wave as the Froude number of the left condition increases (with fixed left water depth):

- For left states with $0 < Fr_L < 0.277$ (thick solid magenta line, left plot, Fig. 6(b)) the corresponding right states are characterized by subcritical conditions (green line, right plot, Fig. 6(b)). At each $\mathbf{W}_L$ in this range corresponds only one $\mathbf{W}_R$. If we consider an RP with initial conditions equal to an admissible pair $(\mathbf{W}_L,\ \mathbf{W}_R)$, this RP develops no other wave except the initial contact wave.
- For left states with $0.277 < Fr_L < 1.677$ (dashed magenta lines, left plots, Fig. 6(a) and (b) there is no possibility to develop a contact wave. If we consider an RP with initial conditions equal to an inadmissible pair $(\mathbf{W}_L,\ \mathbf{W}_R)$, the other waves that develop in this case change the condition near the step so as to reach a pair of values in the admissible ranges.

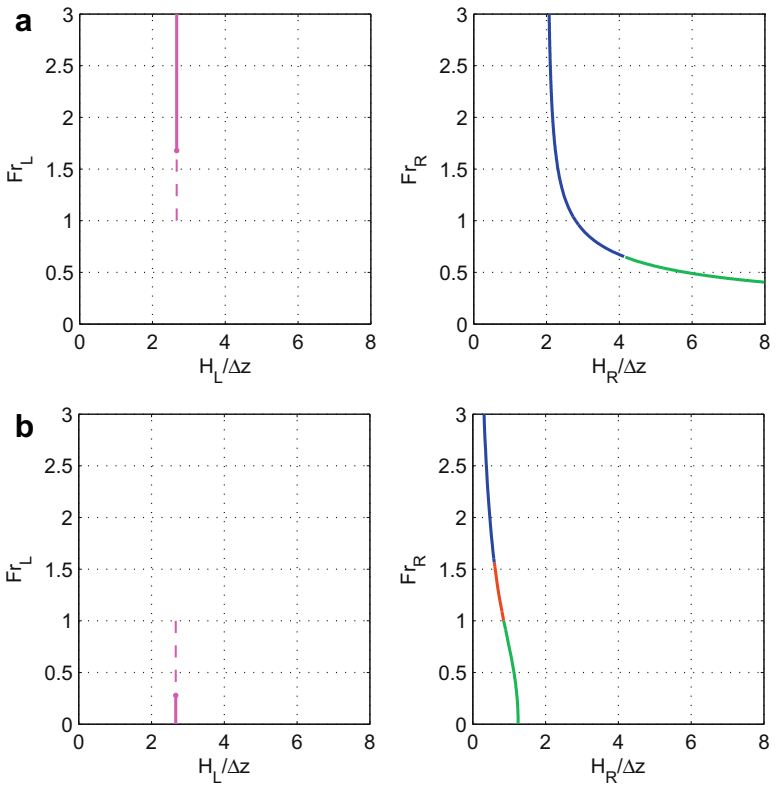

Fig. 6. Possible and admissible left and right states associated with a step contact wave in the case of bed variation of height $\hat{z}_R = 0.75$ m with: (a) supercritical; (b) subcritical $\mathbf{W}_L$ states. Dashed magenta lines: inadmissible left states; thick magenta lines: admissible left states. Otherwise, for meaning of line styles and colors see previous figures.

- For left states with $Fr_L > 1.677$ (thick solid magenta line, left plot, Fig. 6(a)), the right states are characterized by subcritical conditions (green line, right plot, Fig. 6(b)). For each $\mathbf{W}_L$ in this range there is only one $\mathbf{W}_R$. Also in this case, if we consider an RP with initial conditions equal to an admissible pair $(\mathbf{W}_L,\ \mathbf{W}_R)$, this RP develops no other wave except the initial contact wave.

It is worth noticing that a suitable combination of the plots of Fig. 6(a) and (b) leads to the same graphs presented in [4] for the positive step case.

4.3. Negative step

Fig. 7(a) shows the $\mathbf{s}^-_{GHL}$ curves starting from $\mathbf{W}_L$ points as in the previous case, i.e. characterized by a fixed value of $h_L = 2$ m and values of u_L ranging from 0 to 4.43 m/s (which corresponds to Froude numbers ranging from 0 to 1). Fig. 7(b) shows the $\mathbf{s}^-_{GHL}$ curves starting from $\mathbf{W}_L$ points characterized by a fixed value of $h_L = 2$ m and values of u_L greater than 4.43 m/s (corresponding to Froude numbers greater than 1). In both figures, these points are connected by a bold magenta line.

The analysis of these plots can be performed following the same approach outlined for the positive step case. The observations that can be made are the following:

1. In both cases of subcritical (Fig. 7(a)) and supercritical (Fig. 7(b)) states of $\mathbf{W}_L$, there are two distinct branches of the curve: one corresponding to subcritical conditions and the other corresponding to supercritical conditions.
2. In Fig. 7(a), the energy principle rules as inadmissible all the subcritical branches of the GHL curves and parts of the supercritical branches (blue lines). The remaining parts are ruled out by the continuation principle (in red). In other words, no solution is admissible in these conditions. This result is somewhat surprising because one would expect that a subcritical right condition may occur at least for a small negative step. This behavior is due to the assumption regarding the pressure distribution over the step (Eq. 21). Thus, in these conditions, the expression (21) we have assumed for D is not correct, as it leads to rather unphysical results. One could overcome the problem by searching for a proper pressure distribution

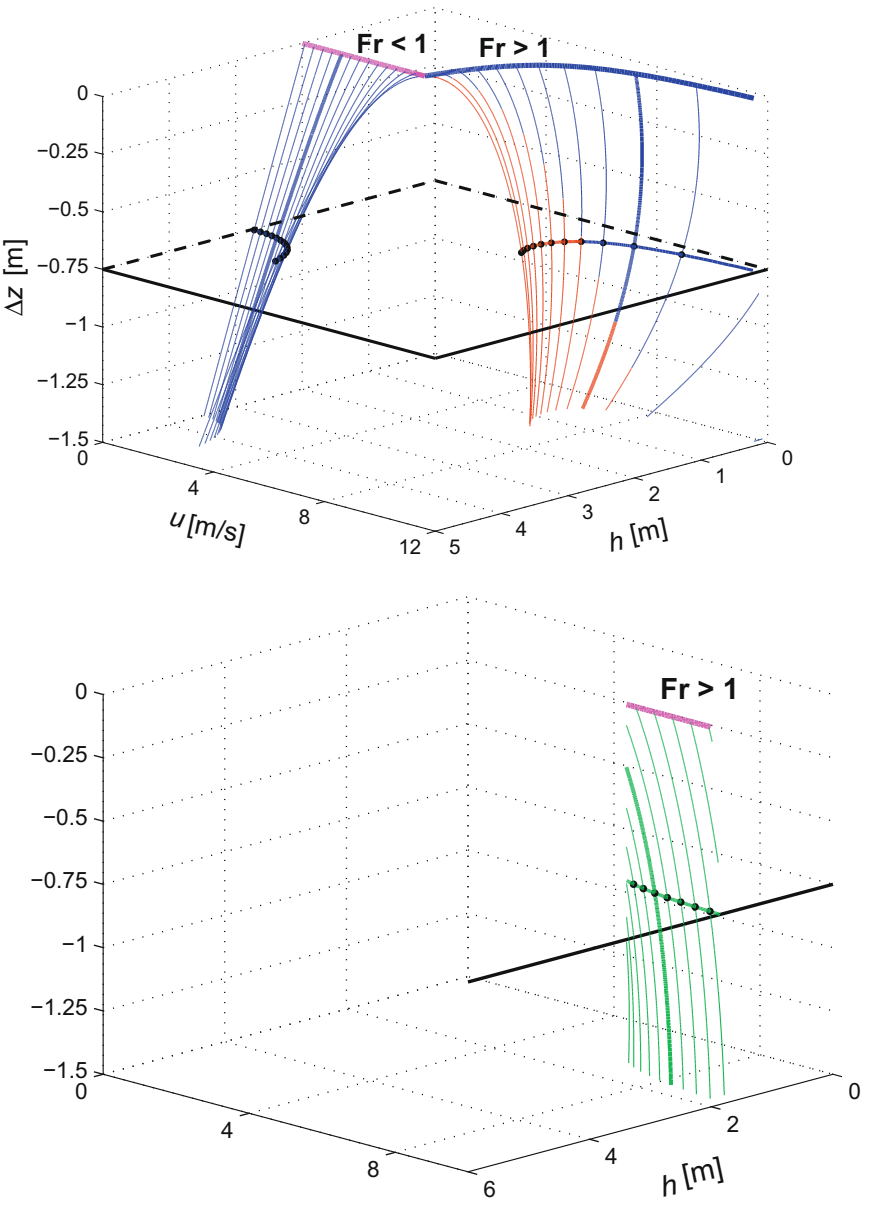

(with the relevant value of D) leading to admissible solutions in this case. However, instead of just trying different assumptions, we believe that a more correct approach will be the derivation of a suitable expression from laboratory experiment. This is left to future work.

3. Let us consider now Fig. 7(b), corresponding to supercritical states $\mathbf{W}_L$ and in particular the $\mathbf{s}_{\overline{GHL}}$ curve plotted with a bold line going from points A to B. Also, consider a negative step of height $\hat{z}_R$. The following cases can be individuated:

   $\hat{z}_R = 0$. This is the case with a null step (horizontal bed condition). There are two possible solutions: the unchanged subcritical condition (point A) and the subcritical condition of point B corresponding to a standard hydraulic jump.

   $\hat{z}_R < 0$. For certain ranges of $\mathbf{W}_L$ both a subcritical and a supercritical admissible state exist: in a complete Riemann Problem over the step, the actual state on the right of the step is determined by the wave that develops downstream of the step.

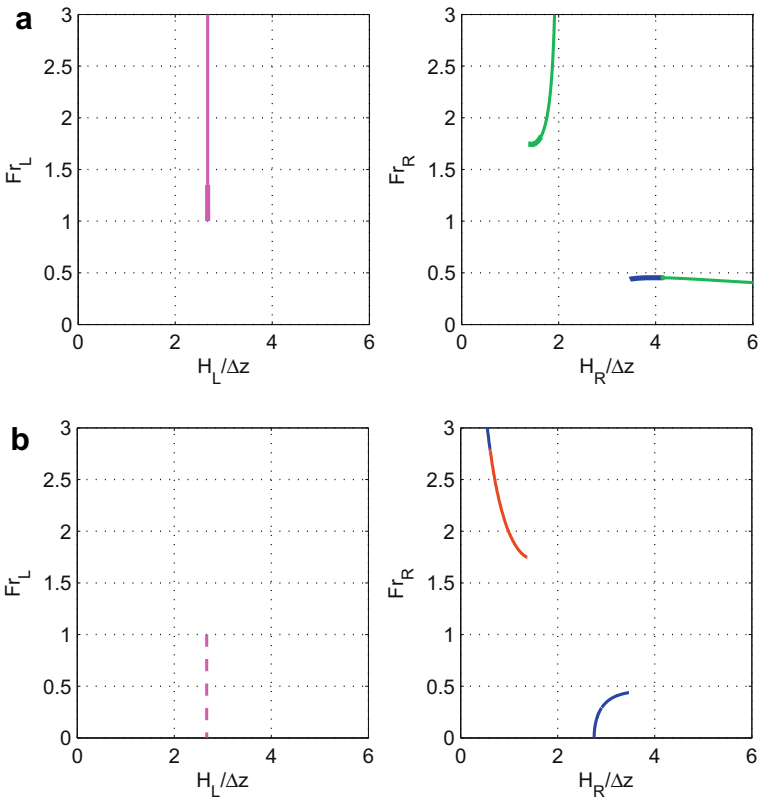

Fig. 8. Possible and admissible left and right states associated to a step contact wave in case of bed variation of height $\hat{z}_R = -0.75$ m with: (a) supercritical; (b) subcritical $\mathbf{W}_L$ states. Dashed magenta lines: unadmissible left states; solid magenta lines: admissible left states. Thick lines: one admissible solution; thin lines: two admissible solutions. Otherwise, for meaning of line styles and colors see previous figures.

4. Let us consider the case with $\hat{z}_R = -0.75$ m: the set of intersections of the $\mathbf{s}_{\overline{GRL}}$ curves with the plane $\hat{z}_R$ is shown in the right plots of Fig. 8(a) and (b) for the subcritical and the supercritical cases, respectively. The colors and the styles of the lines have the same meaning as in previous figures: admissible states in green; states ruled out by the energy principle in blue; states ruled out by the continuation principle in red. In the left graphs, the lines of the possible states on the left of the step are shown: the dashed lines represent states that are inadmissible because there are no intersections with the given step. We consider now what happens to the contact wave as the Froude number of the left state increases (with fixed left water depth):
   - For left states with $0 < Fr_L < 1$ (dashed magenta line, left plot, Fig. 8(b)) there is no possibility for a contact wave to develop. If we consider an RP with initial conditions equal to an inadmissible pair ($\mathbf{W}_L$, $\mathbf{W}_R$), the other waves that develop change the conditions near the step so that a new pair of values in the admissible ranges is reached.
   - For left states with $1 < Fr_L < 1.350$ (thick solid magenta line, left plot, Fig. 8(a)), there is a single admissible right state.
   - For left states with $Fr_L > 1.350$ (solid magenta line, left plot, Fig. 8(a)), there are two distinct right states.

It is again worth noticing that a suitable combination of the plots of Fig. 8(a) and (b) gives the same graphs presented in [4] relating to the negative step case (or, equivalently, since [4] only consider positive steps, to the case of negative velocities).

5. The numerical algorithm for the Step Riemann Problem

In the previous chapter, we have focused on the characterization of the step GHL. Here, we move on a broader view and extend our attention to the numerical solution of the complete SRP, which is the other important goal of this paper. In particular, we want to develop a simple, fast and accurate algorithm able to evaluate, in presence of a step at the boundary between two computational cells, a proper numerical flux to be employed in any efficient SW finite-volume code. Before describing the philosophy and the details of the algorithm, we need to describe briefly the structure of the solution of the SRP.

5.1. The structure of the SRP solution

We look for the general solution of the following problem:

$$\begin{cases} \frac{\partial \mathbf{U}}{\partial t} + \frac{\partial}{\partial x}\mathbf{F}(\mathbf{U}) + \mathbf{H}\frac{\partial \mathbf{U}}{\partial x} = 0 \\ \mathbf{U}(x,0) = \begin{cases} \mathbf{U}_L & \text{if} \quad x < 0 \\ \mathbf{U}_R & \text{if} \quad x > 0 \end{cases} \end{cases} \tag{60}$$

We recall here the results of the eigenstructure analysis of this hyperbolic system (9) presented in Section (2.2.1) and in Appendix A:

- The system presents three eigenvalues (Eq. 11).
- The characteristic field associated with $\lambda^2 = 0$ is linearly degenerate and presents a contact wave whose features are described in detail in Section 4. The relation valid across this wave is the GRH relation expressed by Eq. (24).
- The characteristic fields associated with the other two eigenvalues (λ^1, λ^3) are genuinely non-linear and therefore the corresponding waves (hereafter referred to as *1-wave* and *3-wave*, respectively) can be either shocks, characterized by Eq. (17) or rarefactions, characterized by Eqs. (77) and (78).

Demonstration of the existence and uniqueness of the solution of (60) under the constraints introduced in Section 4 can be found in [4]. Fig. 9 shows an example of a wave structure developing in an SRP. In this case the *1-wave* is a rarefaction propagating to the left while the *3-wave* is a shock propagating to the right. As a consequence, there are two intermediate states $\mathbf{U}_1$ and $\mathbf{U}_2$, to the left and right side of the bed step, respectively. Henceforth, the solution of an SRP will be labeled using the initials of the different waves encountered moving from left to right in the phase plane, using S for Shock, B for Bottom step, and R for Rarefaction. The wave pattern is thus named RBS from Rarefaction – Bottom step – Shock.

The unknowns of this problem are the conserved variable in fields 1 and 2, see Fig. 9, (for a total of 4 unknowns) plus the number of shock speeds (when the wave structure of the solution contains shocks). Therefore, the number of unknowns ranges generally from 4 to 6. Once the wave structure is determined, the exact solution to this problem can be found by solving a nonlinear system of equations constituted by the relations associated with each wave present in the solution. This system presents multiple possible solutions. The only admissible one can be determined by considering the constraints introduced in Section 4. It is clear that an algorithm that searches iteratively for a possible solution and then checks its admissibility is certainly achievable but computationally very heavy.

5.2. A two-step numerical solver

The main idea underlying our numerical strategy is the following:

- To find a good approximate solution to the SRP able to identify the actual wave structure of the solution.
- To write the relevant nonlinear system and use a Newton–Rhapson iterative method to solve the system, up to the exact solution, starting from the approximate values obtained from the approximate SRP solver.

Thus, the approximate solution of the SRP can be seen as a *predictor* step, while the solution of the nonlinear system corresponding to the relevant wave structure, as a *corrector* step. The success of this predictor–corrector strategy relies on the quality of the approximate SRP solver used in the predictor phase: the nearer the approximate solution is to the exact one, the fewer are the iterations required for the iterative procedure to converge to the exact solution.

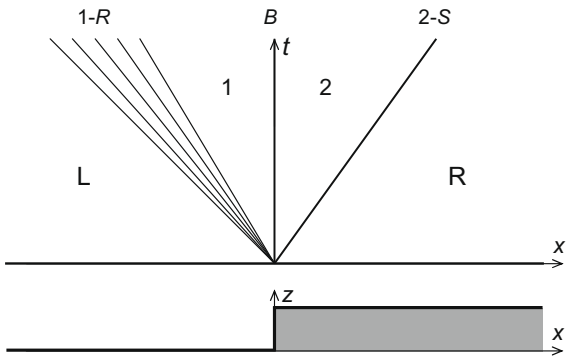

Fig. 9. RBS wave pattern (Rarefaction – Bottom step – Shock). Field labeling: L, R for Left and Right states, numbers for intermediate states.

Clearly, a good predictor solution can be obtained only by considering properly the effect of the bed step. The choice to use a well-balanced solver, i.e. a solver that considers the influence of the step directly in the development of the solution, is almost compulsory. Another advisable property should be the possibility to impose the needed constraints at an early stage of the process and not at the end of it. Therefore, we borrowed the Generalized Roe solver developed in [18] for the mobile-bed case and adapted it for the fixed bed case. In the following section we will present only the essential features of this solver, as well as the novel parts specific to this work, referring the reader to the original work [18] for details on the philosophy that underlies this approach.

5.2.1. The predictor step: the generalized roe solver

The Generalized Roe (GR) solver approximates (60) with the following linear RP:

$$\left.\begin{aligned} &\tfrac{\partial \widehat{\mathbf{U}}}{\partial t} + \widetilde{\mathbf{J}}(\mathbf{U}_L, \mathbf{U}_R)\tfrac{\partial \widehat{\mathbf{U}}}{\partial x} = 0 \\ &\widehat{\mathbf{U}}(x,0) = \begin{cases} \mathbf{U}_L & \text{if} \quad x < 0 \\ \mathbf{U}_R & \text{if} \quad x > 0 \end{cases} \end{aligned}\right\} \tag{61}$$

where $\widetilde{\mathbf{J}}(\mathbf{U}_L,\ \mathbf{U}_R)$ is a constant matrix to be determined by imposing proper conditions, namely:

$$\widetilde{\mathbf{J}}(\mathbf{U}_L, \mathbf{U}_R) = (\mathbf{A}' + \mathbf{A}'')\mathbf{B}^{-1} \tag{62}$$

where

$$\mathbf{A}'(\mathbf{W}_R - \mathbf{W}_L) = \mathbf{F}(\mathbf{U}_R) - \mathbf{F}(\mathbf{U}_L) \tag{63a}$$

$$\mathbf{A}''(\mathbf{W}_R - \mathbf{W}_L) = -\mathbf{D} \tag{63b}$$

$$\mathbf{B}(\mathbf{W}_R - \mathbf{W}_L) = (\mathbf{U}_R - \mathbf{U}_L) \tag{63c}$$

Matrices $\mathbf{A}'$ and $\mathbf{B}$ can be determined as Jacobian matrices, with respect to the primitive variables $\mathbf{W} = (h, u, z)$, of the fluxes and of the conserved variable respectively, evaluated for suitable averaged value of the primitive-variable $\widetilde{\mathbf{W}}$:

$$\mathbf{A}' = \frac{\partial \mathbf{F}}{\partial \mathbf{W}}\bigg|_{\widetilde{\mathbf{W}}} = \begin{pmatrix} 0 & 1 & 0 \\ g\tilde{h} - \tilde{u}^2 & 2\tilde{u} & 0 \\ 0 & 0 & 0 \end{pmatrix} \tag{64}$$

$$\mathbf{B} = \frac{\partial \mathbf{U}}{\partial \mathbf{W}}\bigg|_{\widetilde{\mathbf{W}}} = \begin{pmatrix} 1 & 0 & 0 \\ \tilde{u} & \tilde{h} & 0 \\ 0 & 0 & 1 \end{pmatrix} \tag{65}$$

where

$$\tilde{h} = \frac{h_L + h_R}{2}; \quad \tilde{u} = \frac{u_L\sqrt{h_L} + u_R\sqrt{h_R}}{\sqrt{h_L} + \sqrt{h_R}} \tag{66}$$

while

$$\mathbf{A}'' = \begin{pmatrix} 0 & 0 & 0 \\ 0 & 0 & g\left(h_K - \frac{|z_R - z_L|}{2}\right) \\ 0 & 0 & 0 \end{pmatrix} \quad \text{where } K = \begin{cases} L & \text{if } z_L \leqslant z_R \\ R & \text{otherwise} \end{cases} \tag{67}$$

We define $\tilde{\lambda}^m$ the mth eigenvalue of the matrix (62), $\widetilde{\mathbf{R}}^m$ the right eigenvector associated with $\tilde{\lambda}^m$ and $\tilde{\mu}^m$ the wave strength associated to the mth eigenvalue $\tilde{\lambda}^m$ (see Appendix C for detailed expression of these quantities). If we define the vector of the indices of the ordered eigenvalues

$$I = \begin{cases} (1,2,3) & \text{if} \quad \tilde{\lambda}^1 < \tilde{\lambda}^2 < \tilde{\lambda}^3 \quad \Rightarrow \ \tilde{\lambda}^1 < 0 < \tilde{\lambda}^3 \\ (2,1,3) & \text{if} \quad \tilde{\lambda}^2 < \tilde{\lambda}^1 < \tilde{\lambda}^3 \quad \Rightarrow \ 0 < \tilde{\lambda}^1 < \tilde{\lambda}^3 \\ (1,3,2) & \text{if} \quad \tilde{\lambda}^1 < \tilde{\lambda}^3 < \tilde{\lambda}^2 \quad \Rightarrow \ \tilde{\lambda}^1 < \tilde{\lambda}^3 < 0 \end{cases}$$

we can express the solution in fields 1 and 2 in the following way:

$$\mathbf{U}_i = \mathbf{U}_L + \sum_{k=1,i} [\tilde{\mu}\widetilde{\mathbf{R}}]^{I(i)}$$

while the fluxes can be obtained by multiplying on the left the previous expression by **921.044166.507Tm1TT161Tf1.61.6on-233the34**

5.2.2. An entropy fix for the resonant case

When one of the genuinely non-linear field, namely the *1-wave* or the *3-wave*, is superimposed on the step contact wave, we have the resonance phenomenon: a composite wave structure consisting of a rarefaction with a sonic point situated on one of the sides of the step contact wave (see some examples in Section 6) appears in the solution of the step RP.

It is well-known that any Roe solver, since it is based only on discontinuous solutions, leads to unentropic results in the case of sonic rarefactions. Therefore, the GR solver presented in the previous section suffers, in the case of resonance conditions, from the same drawback as in any other sonic conditions. In this particular case, the implementation of the classical Harten and Hyman [9] entropy fix has been found to be extremely complicated and computationally expensive. Therefore, we adopted an extremely simple fix suggested by the analysis presented in Section 4.

In a resonant case, the GR solver gives a solution with a supercritical condition on one side of the step, and a subcritical condition on the other. With reference to Figs. 5(a) and (b) and 7(a) and (b), this solution corresponds to points belonging to different branches of the GHL curves. This condition is possible but, owing to the continuation principle (or the monotonicity criterion) it is not admissible. Therefore, in order to overcome these unentropic conditions, we impose that on one of the two sides of the step contact wave, flow conditions are critical. But on which side must this condition be set? From Figs. 6 and 8(a) and (b) it is possible to deduce that admissible conditions with $Fr = 1$ may exist only on the right of a positive step (Fig. 6(b)), or on the left of a negative step (Fig. 8(a)). In both cases, we have critical conditions on the side of the step with higher elevation. Therefore, our fix consists in setting critical conditions on the higher side of the step. Recalling that our problem has 4 unknowns (depth and velocity on either side of the step) and considering that the previous condition gives one relation, we need three other relations to close the problem. Two of them derive from the step GRH relations (Eq. 23) while, for the last, we assume that a rarefaction connects the state on the higher side of the step (which could be left or right) to the corresponding initial state of the Riemann Problem (i.e., $\mathbf{U}_L$ or $\mathbf{U}_R$, respectively); the relevant equation is therefore the flat-bed RI relation.

It should be noticed that such a fix does not use a modified version of the original Roe solver but it solves an SRP with an approximated wave structure. Therefore it gives the exact solution when the actual wave structure matches the assumed one; otherwise it provides only approximated solutions. In any case, it is able to rule out inadmissible conditions, and therefore succeeds in the main objective of the predictor step: providing the corrector step with the exact wave structure and a good initial solution.

5.2.3. The corrector step

Once the approximated solution is evaluated, it is possible to determine the actual wave structure of the RP solution from a comparison of the celerity of the 1- and 3-waves evaluated in the fields before and after the wave itself:

$$1\text{-}wave \rightarrow \begin{cases} \text{if} \quad \lambda_1^1 < \lambda_L^1 & \Rightarrow \text{Rarefaction} \\ \text{if} \quad \lambda_1^1 > \lambda_L^1 & \Rightarrow \text{Shock} \end{cases} \tag{69}$$

$$3\text{-}wave \rightarrow \begin{cases} \text{if} \quad \lambda_2^3 < \lambda_R^3 & \Rightarrow \text{Rarefaction} \\ \text{if} \quad \lambda_2^3 > \lambda_R^3 & \Rightarrow \text{Shock} \end{cases} \tag{70}$$

where λ_j^i is the ith eigenvalue evaluated in the jth field (with reference to Fig. 9 for fields labeling).

It is possible now to write the system of equations that defines the full SRP and in particular to determine the number of unknowns of such system. Considering the example shown in Fig. 9, the *predictor* solution would provide an estimation of the intermediate states $\mathbf{U}_1$ and $\mathbf{U}_2$ and would therefore tell us that the structure is RBS with a total of 5 unknowns, namely $(h_1,\ u_1,\ h_2,\ u_2,\ s_2)$. The Corrector Step (CS) would solve the following relevant system:

$$u_L + 2\sqrt{gh_L} = u_1 + 2\sqrt{gh_1} \tag{71a}$$

$$h_1 u_1 = h_2 u_2 \tag{71b}$$

$$h_1 u_1^2 + \frac{1}{2} g h_1^2 = h_2 u_2^2 + \frac{1}{2} g h_2^2 + D \tag{71c}$$

$$h_R u_R - h_2 u_2 = s_2 (h_R - h_2) \tag{71d}$$

$$(h_R u_R^2 + \frac{1}{2} g h_R^2) - (h_2 u_2^2 + \frac{1}{2} g h_2^2) = s_2 (h_R u_R - h_2 u_2) \tag{71e}$$

where Eq. (71a) expresses the constancy of the Riemann Invariant $\left(u_L + 2\sqrt{gh_L}\right)$ across the 1-rarefaction connecting $\mathbf{U}_L$ to $\mathbf{U}_1$, Eqs. (71b) and (71c) express the step GRH relations (18–22) relating the states $\mathbf{U}_1$ and $\mathbf{U}_2$, and Eqs. (71d) and (71e) are the flat-bed RH Eqs. (15) and (16) across the right-moving 2-shock, relating the states $\mathbf{U}_2$ and $\mathbf{U}_R$.

The system is then solved with an iterative Newton–Raphson method in terms of the primitive variables starting from the initial guess deriving from the predictor step. Iterations stop at the required accuracy, which can be set by the user to the value that is considered the optimal trade-off between accuracy and computational cost.

Finally, the numerical fluxes before and after the step are:

$$\mathbf{F}^*_{0^-} = \begin{cases} \mathbf{F}_1^{GR+CS} & \text{if } \tilde{\lambda}^1 < \tilde{\lambda}^2 < \tilde{\lambda}^3 \\ \mathbf{F}_L & \text{if } \tilde{\lambda}^2 < \tilde{\lambda}^1 < \tilde{\lambda}^3 \\ \mathbf{F}_2^{GR+CS} & \text{if } \tilde{\lambda}^1 < \tilde{\lambda}^3 < \tilde{\lambda}^2 \end{cases}; \quad \mathbf{F}^*_{0^+} = \begin{cases} \mathbf{F}_2^{GR+CS} & \text{if } \tilde{\lambda}^1 < \tilde{\lambda}^2 < \tilde{\lambda}^3 \\ \mathbf{F}_1^{GR+CS} & \text{if } \tilde{\lambda}^2 < \tilde{\lambda}^1 < \tilde{\lambda}^3 \\ \mathbf{F}_R & \text{if } \tilde{\lambda}^1 < \tilde{\lambda}^3 < \tilde{\lambda}^2 \end{cases} \tag{72}$$

where the superscript $GR + CS$ indicates that the fluxes result from the two steps, namely the Generalized Roe step (GR) plus the Corrector Step (CS).

6. Numerical applications

In order to check the effectiveness of the proposed approach, we considered a series of SRPs whose exact solution can be obtained by an inverse procedure (see. e.g. [2,17]). The domain of the tests is divided into N computational cells of a constant size Δx. The interval of the ith cell is defined by $[x_{i-1/2}, x_{i+1/2}]$ where $x_{i+1/2} = x_0 + i\Delta x$ and the position of the center of the cell x_i is defined by $(i - 1/2)\Delta x$. Let Δt be the time step and $t^n = n\Delta t$ a generic time. We indicate with $\mathbf{U}_i^n$ the cell-average value of the solution $\mathbf{U}(x,t)$ for the ith cell at time t^n. The bed step is positioned on the left side of the Mth cell, i.e. it is at position $x_{M+1/2} = 0$. The update formula for cell M and $M + 1$ is the following:

$$\mathbf{U}_M^{n+1} = \mathbf{U}_M^n + \frac{\Delta t}{\Delta x}\left(\mathbf{F}^*_{M-1/2} - \mathbf{F}^*_{(M+1/2)^-}\right)$$
$$\mathbf{U}_{M+1}^{n+1} = \mathbf{U}_{M+1}^n + \frac{\Delta t}{\Delta x}\left(\mathbf{F}^*_{(M+1/2)^+} - \mathbf{F}^*_{M+3/2}\right)$$

where $\mathbf{F}^n_{M\pm1/2}$ are evaluated with a standard solver while $\mathbf{F}^*_{(M+1/2)^\pm}$ are given by a bed step solver. For all the other cells, the update formula is the usual one (see flowchart in Fig. 10).

To evaluate the numerical fluxes at cell interfaces without bottom discontinuities, we used a classical Roe approach, while in the case with bed discontinuities two different approaches were tested for comparison purposes. The first method consists in using the full two-step approach ($GR + CS$): fluxes $\mathbf{F}^*_{(M+1/2)^\pm}$ are evaluated by means of (72) in which $\mathbf{F}_L = \mathbf{F}_M$ and $\mathbf{F}_R = \mathbf{F}_{M+1}$. The second is obtained simply using the numerical fluxes resulting from the predictor approach plus the resonance fix (GR), i.e. by using scheme (72) where the fluxes $\mathbf{F}_i^{GR}$ (Eq. 68) are used instead of $\mathbf{F}_i^{GR+CS}$. This was done in order to check whether or

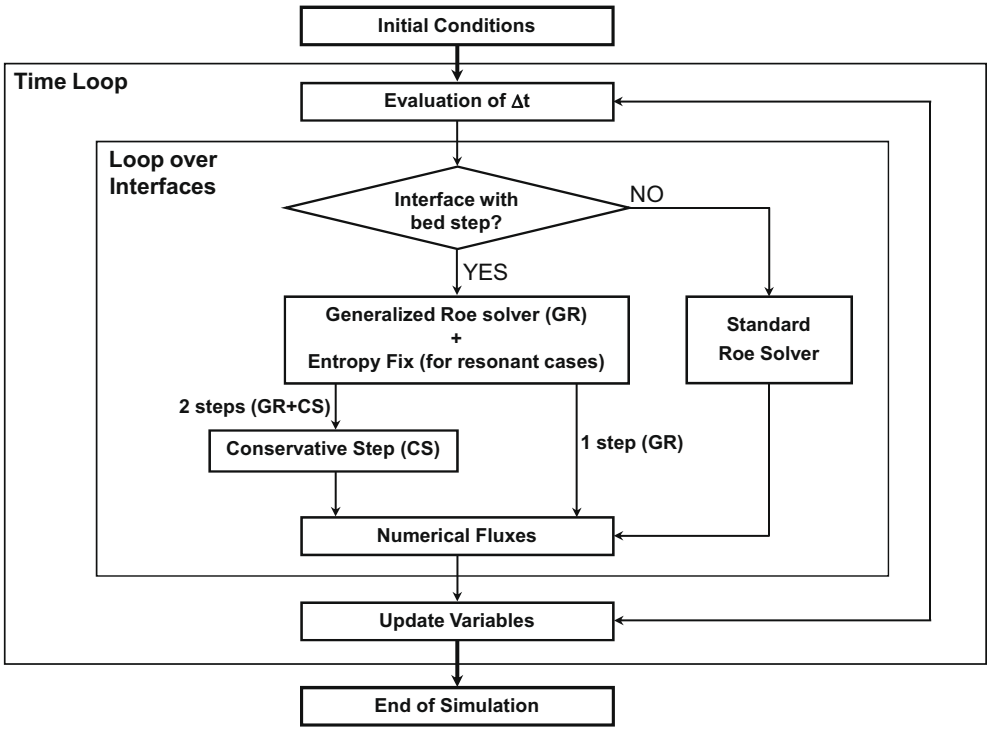

Fig. 10. Flowchart of the numerical algorithm.

Table 1
List of the initial left and right conditions of the test cases.

Test	Left			Right		
	h_L (m)	u_L (m/s)	z_L (m)	h_R (m)	u_R (m/s)	z_R (m)
RBS	5.0	0	0	0.9966	0	1
RBR	8.0	−2.0	0	5.0	7.1704	1
SBS	4.0	4.7500	0	1.0838	−2.1854	1
RRBR	6.0	−16.0	0	8.0	0	1
SBRS	4.0	7.0	0	1.0299	7.1290	1

not (or, to what extent) the predictor solution can be used when quick (but less accurate) simulations are needed for practical purposes.

All the numerical solutions presented here have been obtained using a grid of 2000 cells; left and right initial conditions for each problem are shown in Table 1. In the corrector step, the L_∞ relative error required to stop the iterations was set to 10^{-9}. Here we present a systematic comparison between the exact solution, the numerical solution resulting from the predictor step only (GR) and the full algorithm ($GR + CS$). These results are shown in Figs. 11–13; for clarity, only a fraction of the 2000 computational points is represented.

Test RBS: This case corresponds to a dam break over wet bed, i.e. initial conditions with left and right velocities equal to zero and different water depths (with $h_L > h_R$). In this case, the solution of the Riemann Problem, is constituted by a left moving 1-Rarefaction, the bottom step discontinuity and a right-moving 2-Shock (assuming that the left rarefaction does not span across the x-axis). A sketch of the wave structure is shown in Fig. 9. Results are shown in Fig. 11(a). It can be noticed that the numerical results obtained using the two approaches (GR) and ($GR + CS$), are nearly identical and both indistinguishable from the exact solution

Test RBR: In this case we have two rarefactions moving away from the step, one to the left and one to the right. Thus, the solution of the Riemann Problem is given by a left-propagating 1-Rarefaction, the bottom step discontinuity and a right-propagating 2-Rarefaction. Results are shown in Fig. 11(b). Again, the numerical results obtained using the two approaches (GR) and ($GR + CS$) are both indistinguishable from the exact solution.

Test SBS: In this case two shocks are moving away from the bottom step in opposite directions, and the solution of the Riemann Problem is therefore given by a left-propagating 1-Shock, the bottom step discontinuity and a right-propagating 2-Shock. Results are shown in Fig. 12(a). As in the two previous cases, the two approaches (GR) and ($GR + CS$) give numerical results in perfect agreement with the exact solution.

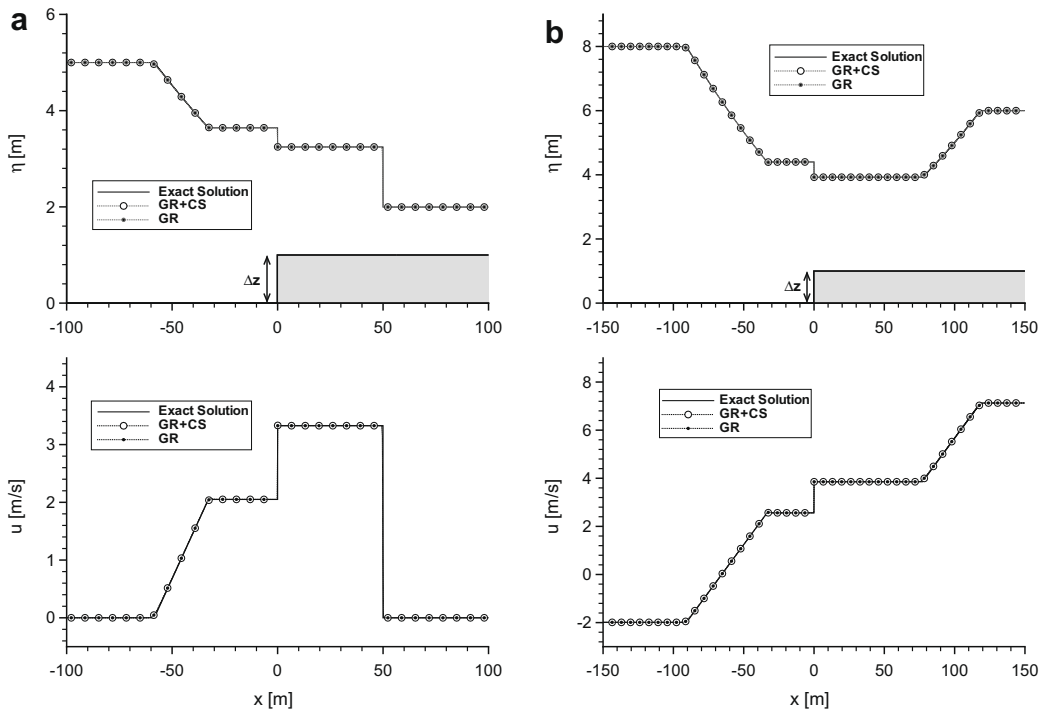

Fig. 11. Comparison between exact and numerical solutions (top: $\eta = z + h$, bottom: u) at time $t = 8$ s, in case: (a) RBS, and (b) RBR.

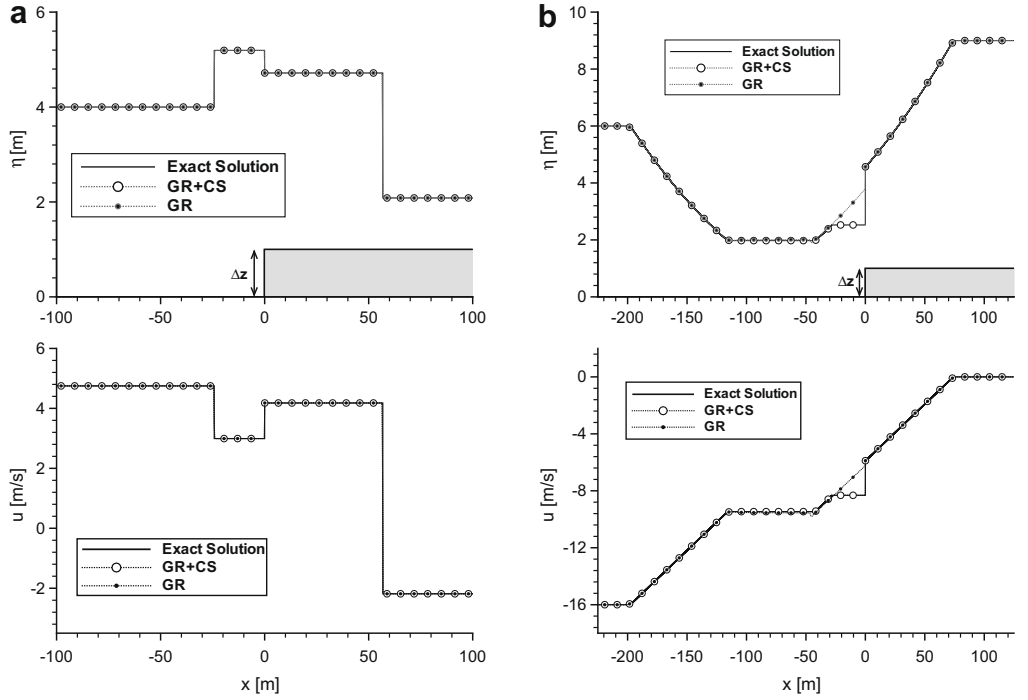

Fig. 12. Comparison between exact and numerical solutions (top: $\eta = z + h$, bottom: u) at time $t = 8$ s, in case: (a) SBS, and (b) RRBR.

Test RRBR: This differs from the previous tests because of the presence of a resonant condition. The wave pattern is given by a 1-Rarefaction propagating to the left, a left-propagating 2-Rarefaction and a composite wave made up of a step contact wave and a right-propagating 2-Rarefaction spanning from the right state to the step. It must be noted that, in accordance with the theory developed so far in the paper, flow conditions are critical to the right side of the step (i.e., the side with the highest bottom elevation), while on the left side flow conditions are those given by the step GRH relationship. Results for this problem are shown in Fig. 12(b). Contrary to the previous cases, there are evident differences here between the two numerical solutions. Using the predictor fluxes (GR), the model clearly fails to correctly simulate the flow to the right of the bottom step. This shows that the fix we have introduced, although successful in avoiding unphysical flow conditions, does not lead to the exact solution. On the other hand, using the two-step approach ($GR + CS$), the model converges to the exact solution. Therefore, the predictor achieves its primary aim, which is to provide an approximate solution that allows the corrector step to converge to the exact solution.

Test SBRS: In this case, as in the previous one, the resonance phenomenon affects the step RP and the flow conditions are critical to the right side of the step (i.e. the side with the highest bottom elevation). The flow is everywhere from left to right, and the wave structure can be easily deduced from Fig. 13, where numerical and analytical solutions are presented. As can be seen from the figure, the wave structure is clearly not well predicted by the predictor step (GR) alone, but correctly captured by using the full algorithm ($GR + CS$), which gives numerical results identical to the exact solution.

6.1. Overall considerations

From the analysis of the previous numerical results it is possible to draw some general observations regarding the proposed algorithm.

1. The full algorithm guarantees high accuracy in any flow conditions. In particular, unlike other approaches (see [4]), no spurious oscillations are present near the step contact wave, either in the elevation or in the velocity values.
2. The accuracy of the solver can be tuned simply by adjusting the tolerance in the corrector phase. This gives it a great flexibility allowing any desired accuracy to be obtained rather easily.
3. The number of iterations necessary in the corrector step is rather limited. In any simulation it did not exceed the value of 3 with the tolerance used in this work; this number can be easily reduced by simply increasing the tolerance, which speeds up the algorithm but reduces the accuracy.
4. The GR solver can be used without the corrector step in any situation except those presenting the resonance phenomenon. In this case at least one iteration is compulsory to obtain a solution with an acceptable approximation.

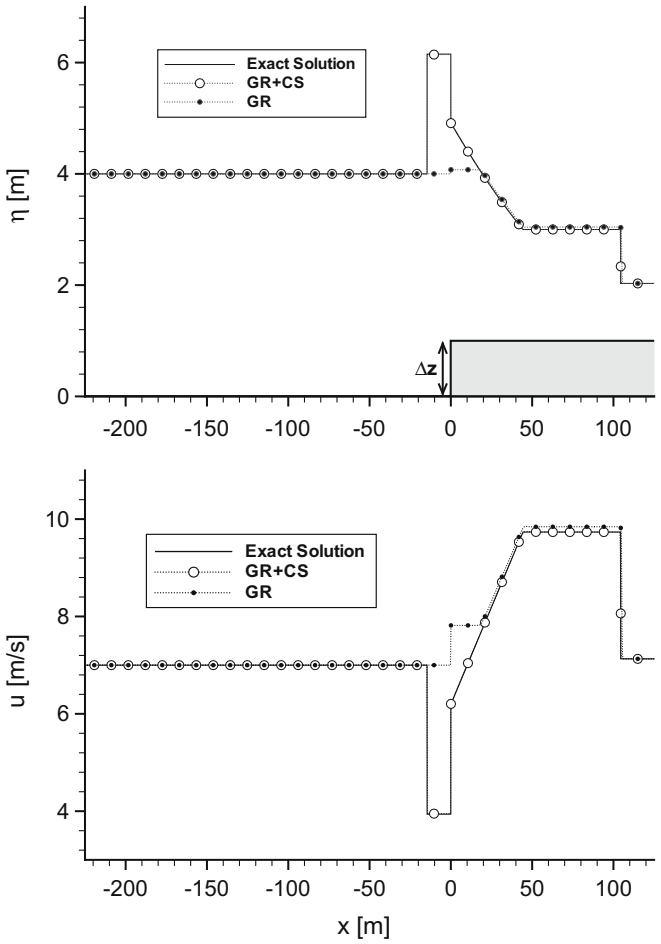

Fig. 13. Comparison between exact and numerical solutions (top: $\eta = z + h$, bottom: u) at time $t = 8$ s for the SBRS case.

5. It must be noted that incorrect solution around the step may affect the correctness of the solution in the whole domain (see Fig. 13). Therefore, the step solver must have at least the same accuracy as the solver used elsewhere.

7. Conclusions

We have presented in this paper the solution of the Riemann Problem for the one-dimensional Shallow Water Equations over a bed discontinuity from the theoretical and a numerical point of view. A deep analysis of the features of the contact wave in nonconservative systems allowed us to show that unlike in standard conservative systems, RIs are generally not constant across nonconservative contact discontinuities characterized by a speed independent from the variables of the problem. The application of this general result to the extended 1D SW system demonstrates that across the step contact wave the energy is not conserved. In this way, we have provided a comprehensive mathematical description of the problem that does not contradict the physical evidence regarding energy conservation and thus overcomes the contradictions so far present in the literature that are discussed in the introduction. A thorough analysis of the mathematical properties of the step contact waves, complemented by several figures representing the GRH relations, allowed us to obtain a clear and direct characterization of the features of this wave.

From a numerical point of view, we have presented an SRP solver whose accuracy can be extended up to the exact solution without excessive numerical burden. Its use, in conjunction with a standard first order Roe scheme for a horizontal bed, furnished numerical results remarkably near to the exact ones in a series of test cases involving different types of SRPs. This solver can also be easily embedded in any finite-volume, Godunov method.

Even though the theoretical and numerical framework for solving the SRP in a one-dimensional context has been achieved, a large amount of work must now be devoted to collecting experimental data, in order to find a more correct relation expressing the step thrust term (20), and to verifying to what extent the SW approach can be representative of the actual

physical problem. Moreover, it could be interesting to obtain the thrust term from suitable averaging of the fully 2D Reynolds equations (or possibly of the simplified 2D Euler equations) and compare systematically the results that can be obtained from different levels of approximations (for example in the way outlined by [14] for the case of a smooth obstacle). This is the target of our future work on this topic.

Appendix A. Eigenstructure analysis of the SW system in terms of primitive variables

Considering system (7), its quasi-linear form in terms of primitive variables $\mathbf{W}^T = (h, u, z)$ reads:

$$\mathbf{B}\frac{\partial \mathbf{W}}{\partial t} + (\mathbf{J_W} + \mathbf{HB})\frac{\partial \mathbf{W}}{\partial x} = 0 \tag{73}$$

where

$$\mathbf{B} = \frac{d\mathbf{U}}{d\mathbf{W}} = \begin{bmatrix} 1 & 0 & 0 \\ u & h & 0 \\ 0 & 0 & 1 \end{bmatrix}, \quad \mathbf{J_W} = \frac{d\mathbf{F}}{d\mathbf{W}} = \begin{bmatrix} u & h & 0 \\ u^2 + gh & 2hu & 0 \\ 0 & 0 & 0 \end{bmatrix}$$

Multiplying on the left by $\mathbf{B}^{-1}$, system (73) can be rewritten as:

$$\frac{\partial \mathbf{W}}{\partial t} + \left(\mathbf{B}^{-1}\mathbf{J_W} + \mathbf{B}^{-1}\mathbf{HB}\right)\frac{\partial \mathbf{W}}{\partial x} = 0$$

The eigenvalues of this equations are given by the following relation:

$$\det|\mathbf{B}^{-1}\mathbf{J_W} + \mathbf{B}^{-1}\mathbf{HB} - \lambda\mathbf{I}| = 0$$

while the right eigenvalues are given by

$$(\mathbf{B}^{-1}\mathbf{J_W} + \mathbf{B}^{-1}\mathbf{HB})\widetilde{\mathbf{R}}^k = \lambda_k \widetilde{\mathbf{R}}^k \tag{74}$$

As proved in [18], the previous eigenvalues are the same as can be obtained from the eigenstructure analysis in terms of the conserved variables (Eq. 11); moreover, the relation between the respective eigenvectors is:

$$\mathbf{R}^k = \mathbf{B}\widetilde{\mathbf{R}}^k \tag{75}$$

In detail, the eigenvectors are:

$$\widetilde{\mathbf{R}}^1 = \begin{bmatrix} 1 \\ -\frac{1}{h}\sqrt{gh} \\ 0 \end{bmatrix}; \quad \widetilde{\mathbf{R}}^2 = \begin{bmatrix} 1 \\ -\frac{1}{h}u \\ -\frac{1}{gh}(gh - u^2) \end{bmatrix}; \quad \widetilde{\mathbf{R}}^3 = \begin{bmatrix} 1 \\ \frac{1}{h}\sqrt{gh} \\ 0 \end{bmatrix}$$

As far as the ICs are concerned, from Eq. (31) we have:

$$\frac{d\mathbf{s}^k}{d\mathbf{W}}\frac{d\tilde{\mathbf{s}}^k}{d\xi} = \mathbf{B}\frac{d\tilde{\mathbf{s}}^k}{d\xi}$$

considering Eqs. (75) and (32) becomes:

$$\mathbf{B}\frac{d\tilde{\mathbf{s}}^k}{d\xi} = \mathbf{B}\widetilde{\mathbf{R}}^k \;\Rightarrow\; \frac{d\tilde{\mathbf{s}}^k}{d\xi} = \widetilde{\mathbf{R}}^k$$

This relation expresses the formal equivalence of the ICs in terms of primitive variables $\tilde{\mathbf{s}}^k$ with the ICs in terms of conserved variables $\mathbf{s}^k$. The ICs associated with the step contact wave $\lambda_2 = 0$ can be obtained by integrating the previous expression:

$$\tilde{\mathbf{s}}^2(\xi) = \begin{bmatrix} h(\xi) \\ u(\xi) \\ z(\xi) \end{bmatrix} = \begin{bmatrix} h_L + \xi \\ \frac{h_L u_L}{\xi + h_L} \\ z_L - \xi - \frac{(h_L u_L)^2}{2g}\frac{1}{(\xi + h_L)^2} + \frac{(u_L)^2}{2g} \end{bmatrix} \tag{76}$$

It can be noticed that the second equation derives from the mass conservation principle $uh = const = q$, where q is the discharge per unit width, while the third equation derives from the energy conservation principle $h + \frac{u^2}{2g} + z = const = E$ where E is the energy per unit weight of fluid. The first Riemann invariant associated with the λ_2-field is:

$$\frac{dh}{\widetilde{R}_1^2} = \frac{du}{\widetilde{R}_2^2}$$
$$\frac{dh}{1} = \frac{du}{-\frac{1}{h}u}$$

which, after some manipulations gives

$$hu = const \tag{77}$$

The second equation is

$$\frac{dh}{\widetilde{R}_1^2} = \frac{dz}{\widetilde{R}_3^2}$$
$$\frac{dh}{1} = \frac{dz}{-\frac{1}{gh}(gh - u^2)}$$

which, after some manipulations, and with the use of the other invariant, gives

$$h + \frac{u^2}{2g} + z = const \tag{78}$$

Finally, it must be noted that the same RIs could be obtained by performing the same analysis in terms of the conserved variables.

Appendix B. Contact waves in primitive-variable nonconservative systems

Theorem 1 can be also formulated in terms of the primitive variables $\mathbf{W}$. The variation of $(\mathbf{F} - S\mathbf{U} - \mathbf{D})$ along $\tilde{\mathbf{s}}$, with $S_s = \lambda_k$, becomes:

$$\frac{d}{d\xi}(\mathbf{F} - S_s\mathbf{U}) = \frac{d\mathbf{F}}{d\mathbf{W}}\frac{d\tilde{\mathbf{s}}^k}{d\xi} - S_s\frac{d\mathbf{U}}{d\mathbf{W}}\frac{d\tilde{\mathbf{s}}^k}{d\xi} - \frac{d\mathbf{D}}{d\xi} = \mathbf{J}_\mathbf{W}\widetilde{\mathbf{R}}^k - \lambda_k\mathbf{B}\widetilde{\mathbf{R}}^k - \frac{d\mathbf{D}}{d\xi} \tag{79}$$

Multiplying on the left Eq. (74) by $\mathbf{B}$ we obtain:

$$\mathbf{B}\mathbf{B}^{-1}\mathbf{J}_\mathbf{W}\widetilde{\mathbf{R}}^k - \lambda_k\mathbf{B}\widetilde{\mathbf{R}}^k = -\mathbf{B}\mathbf{B}^{-1}H\mathbf{B}\widetilde{\mathbf{R}}^k$$
$$\mathbf{J}_\mathbf{W}\widetilde{\mathbf{R}}^k - \lambda_k\mathbf{B}\widetilde{\mathbf{R}}^k = -\mathbf{H}\mathbf{B}\widetilde{\mathbf{R}}^k$$

In order to have $d(\mathbf{F} - S_s\mathbf{U})/d\xi = 0$, we must set

$$-\mathbf{H}\mathbf{B}\widetilde{\mathbf{R}}^k - \frac{d\mathbf{D}}{d\xi} = 0$$

which, after integrations, gives:

$$-\int_0^\xi \mathbf{H}\mathbf{B}\widetilde{\mathbf{R}}^k d\xi = \mathbf{D}$$

Appendix C. Detailed expression of quantities used in the Step Generalized Roe solver

The eigenvalues of matrix (62) are:

$$\tilde{\lambda}^1 = \tilde{u} - \tilde{c}; \quad \tilde{\lambda}^2 = 0; \quad \tilde{\lambda}^3 = \tilde{u} + \tilde{c} \tag{80}$$

with $\tilde{c} = \sqrt{g\tilde{h}}$, where the averaged primitive values are already defined in (66). The relevant eigenvectors are:

$$\widetilde{\mathbf{R}}^1 = \begin{pmatrix} 1 \\ \tilde{u} - \tilde{c} \\ 0 \end{pmatrix}; \quad \widetilde{\mathbf{R}}^2 = \begin{pmatrix} a_{23} \\ 0 \\ \tilde{u}^2 - \tilde{c}^2 \end{pmatrix}; \quad \widetilde{\mathbf{R}}^3 = \begin{pmatrix} 1 \\ \tilde{u} + \tilde{c} \\ 0 \end{pmatrix} \tag{81}$$

where a_{23} is the component (2,3) of $\mathbf{A}''$ (see 67), namely $g(h_K - |z_R - z_L|/2)$ where $K = L$ if $z_L \leqslant z_R, R$ otherwise. Finally, the wave strengths are:

$$\begin{cases} \tilde{\mu}^1 = \frac{\delta_h\tilde{\lambda}^3 - \delta_{uh}}{2\tilde{c}} - \frac{a_{23}\delta_z}{2\tilde{c}\tilde{\lambda}^1} \\ \tilde{\mu}^2 = \frac{\delta_z}{\tilde{\lambda}^1\tilde{\lambda}^3} \\ \tilde{\mu}^3 = -\frac{\delta_h\tilde{\lambda}^1 - \delta_{uh}}{2\tilde{c}} + \frac{a_{23}\delta_z}{2\tilde{c}\tilde{\lambda}^3} \end{cases} \quad \text{where} \quad \begin{cases} \delta_z = z_R - z_L \\ \delta_h = h_R - h_L \\ \delta_{uh} = h_R u_R - h_L u_L \end{cases} \tag{82}$$

References

[1] F. Alcrudo, F. Benkhaldoun, Exact solutions to the Riemann problem of the shallow water equations with a bottom step, Computers and Fluids 30 (2001) 643–671.

[2] N. Andrianov, Performance of numerical methods on the non-unique solution to the Riemann problem for the shallow water equations, International Journal for Numerical Methods in Fluids 47 (2005) 825–831.
[3] A. Armanini, L. Fraccarollo, G. Rosatti, Two-dimensional simulation of debris flows in erodible channels, Computers and Geosciences 35 (2009) 993–1006.
[4] R. Bernetti, V.A. Titarev, E.F. Toro, Exact solution of the Riemann problem for the shallow water equations with discontinuous bottom geometry, Journal of Computational Physics 227 (2008) 3212–3243.
[5] V.I. Bukreev, A.V. Gusev, V.V. Ostapenko, Breakdown of a discontinuity of the free fluid surface over a bottom step in a channel, Fluid Dynamics 38 (6) (2003) 889–899.
[6] A. Chinnayya, A.Y. LeRoux, N. Seguin, A well-balanced numerical scheme for the approximation of the shallow water equations with topography: the resonance phenomenon, International Journal of Finite Volumes 1 (1) (2004) 1–33.
[7] T. Galloüet, J.M. Hérard, N. Seguin, Some approximate Godunov schemes to compute shallow-water equations with topography, Computers and Fluids 32 (2003) 479–513.
[8] W.H. Hager, R. Bremen, N. Kawagoshi, Classical Hydraulic jump – length of roller, Journal of Hydraulic Research 28 (5) (1990) 591–608.
[9] A. Harten, J.M. Hyman, Self-adjusting grid methods for one-dimensional hyperbolic conservation laws, Journal of Computational Physics 50 (1983) 235–269.
[10] P.G. LeFloch, M.D. Thanh, The Riemann problem for fluid flows in a nozzle with discontinuous cross-section, Preprint NI03024-NPA, Isaac Newton Institute for Mathematical Sciences, University of Cambridge, UK, 2003.
[11] A.Y. LeRoux, Discretisation des termes sources raides dans les probl emes hyperboliques. In: Systemes Hyperboliques: Nouveaux Schemas et Nouvelles Applications, EEcoles CEA-EDF-INRIA 'Problemes Non Lineaires Appliques', INRIA Rocquencourt, France, March 1998.
[12] R.J. LeVeque, Numerical Methods for Conservation Laws, Birkhäusen Verlag, 1992.
[13] R.J. LeVeque, Finite Volume Methods for Hyperbolic Problems, Cambridge University Press, Cambridge, UK, 2002.
[14] B.T. Nadiga, L.G. Margolin, P.K. Smolarkiewicz, Different approximations of shallow fluid flow over an obstacle, Physics of Fluids 8 (8) (1996) 2066–2077.
[15] C.M. Parés, M. Castro, On the well-balance property of Roe's method for nonconservative hyperbolic systems, applications to shallow-water systems, ESAIM:M2AN 38 (5) (2004) 821–852.
[16] C. Parés, Numerical methods for nonconservative hyperbolic systems: a theoretical framework, SIAM Journal of Numerical Analysis 44 (1) (2006) 300–321.
[17] G. Rosatti, L. Fraccarollo, A well-balanced approach for flows over mobile-bed with high sediment-transport, Journal of Computational Physics 220 (2006) 312–338.
[18] G. Rosatti, J. Murillo, L. Fraccarollo, Generalized Roe schemes for 1D two-phase, free-surface flows over a mobile bed, Journal of Computational Physics 227 (2008) 10058–10077.
[19] S.B. Savage, K. Hutter, The motion of a finite mass of granular material down a rough incline, Journal of Fluid Mechanics 199 (1989) 177–215.
[20] J. Smoller, Shock Waves and Reaction–diffusion Equation, second ed., Springer, New York, USA, 1994.
[21] J.J. Stoker, Water Waves, Interscience, NewYork, USA, 1957.
[22] E.F. Toro, Shock-capturing Methods for Free-surface Flows, Wiley and Sons Ltd., 2001.
[23] I. Toumi, A weak formulation of Roe's approximate Riemann solver, Journal of Computational Physics 102 (1992) 360–373.
[24] J.G. Zhou, D.M. Causon, D.M. Ingram, C.G. Mingham, Numerical solution of the shallow water equations with discontinuous bed topography, International Journal for Numerical Methods in Fluids 38 (2002) 769–788.